Quantitative Computed Tomography Based Finite Element Modeling of Normal and Osteoarthritic Knees: *In vivo* Precision and Preliminary Comparisons

A Thesis Submitted to the College of

Graduate Studies and Research

In Partial Fulfillment of the Requirements

For the Degree of Master of Science

In the Department of Mechanical Engineering

University of Saskatchewan

Saskatoon

By

Hanieh Arjmand

Permission to use

In presenting this thesis/dissertation in partial fulfillment of the requirements for a Postgraduate degree from the University of Saskatchewan, I agree that the Libraries of this University may make it freely available for inspection. I further agree that permission for copying of this thesis/dissertation in any manner, in whole or in part, for scholarly purposes may be granted by the professor or professors who supervised my thesis/dissertation work or, in their absence, by the Head of the Department or the Dean of the College in which my thesis work was done. It is understood that any copying or publication or use of this thesis/dissertation or parts thereof for financial gain shall not be allowed without my written permission. It is also understood that due recognition shall be given to me and to the University of Saskatchewan in any scholarly use which may be made of any material in my thesis/dissertation.

Disclaimer

Reference in this thesis/dissertation to any specific commercial products, process, or service by trade name, trademark, manufacturer, or otherwise, does not constitute or imply its endorsement, recommendation, or favoring by the University of Saskatchewan. The views and opinions of the author expressed herein do not state or reflect those of the University of Saskatchewan, and shall not be used for advertising or product endorsement purposes.

Requests for permission to copy or to make other uses of materials in this thesis/dissertation in whole or part should be addressed to:

Head of the Department of Mechanical Engineering

University of Saskatchewan

Saskatoon, Saskatchewan S7N 5A9

Canada

OR

Dean

College of Graduate Studies and Research

University of Saskatchewan

107 Administration Place

Saskatoon, Saskatchewan S7N 5A2

Canada

Abstract

Osteoarthritis (OA) is a debilitating joint disease which affects nearly 85% of the Canadian population over 75 years of age. OA not only affects cartilage, but it also alters subchondral bone (bone underlying cartilage). Altered subchondral bone could be related to OA initiation, progression, and OA-related pain. To help clarify the role of subchondral bone in OA, accurate *in vivo* methods are needed to monitor subchondral bone mechanical property variations in people living with OA. Subject-specific finite element (FE) modeling has potential to investigate the role of mechanical properties of subchondral bone in OA. However, associated precision errors of FE-derived mechanical properties are not known.

The objectives of this study were to 1) develop a subject-specific FE modeling methodology for OA and normal knees, 2) determine the *in vivo* precision of FE-derived stress/strain distributions and stiffness of the proximal tibia, and 3) determine whether FE-derived metrics discriminate normal and OA knees.

Subject-specific FE models were developed for 14 participants (7 OA, 7 normal) with three repeated CT images of knee joint. Von-Mises stress and strain, minimum principal stress and strain, plus structural stiffness outcomes were acquired for each proximal tibia image. Root mean square coefficient of variations (CV%) were used to assess *in vivo* precision of the FE-based outcomes. Comparisons between OA and normal groups were performed using unpaired t-tests for normally distributed outcomes, and Mann-Whitney U-tests for not normally distributed outcomes.

For all the outcomes the average CV% was less than 6.1%. On average, von-Mises stress and minimum principal stress were respectively 65% and 70% higher in OA versus normal knees whereas strain values did not differ. No difference was observed in stiffness values.

Thesis results indicate that FE modeling could be used to precisely quantify and differentiate mechanical property variations in normal and OA knees, *in vivo*. Results suggest that OA and normal bone exhibit dissimilar stress levels but similar strain levels, likely indicating adaptation of bone in response to altered joint mechanics with OA.

Preface

The results of this study were presented at international and local conferences:

- Arjmand, H; Nazemi, M; Kontulainen, SA; Milner, JS; Holdsworth, DW; McLennan, CE; Hazel, D; Talmo, C; Hunter, DJ; Wilson, DR; Johnston, JD; ' Computational modeling of normal and osteoarthritic proximal tibiae: precision and preliminary comparisons of subchondral bone mechanical properties', 9th International workshop on osteoarthritis imaging, June, 2016.

- Arjmand, H; Nazemi, M; Kontulainen, SA; Milner, JS; Holdsworth, DW; McLennan, CE; Hazel, D; Talmo, C; Hunter, DJ; Wilson, DR; Johnston, JD; ' Precision and preliminary comparison of subchondral bone mechanical properties at the proximal tibia from normal and osteoarthritic knees', AAOS/ORS tackling joint disease by understanding crosstalk between cartilage and bone research symposium, April, 2016.

- Arjmand, H; Nazemi, M; Kontulainen, SA; Milner, JS; Holdsworth, DW; McLennan, CE; Hazel, D; Talmo, C; Hunter, DJ; Wilson, DR; Johnston, JD; 'Finite element modeling of proximal tibial stiffness in normal and osteoarthritic knees: *in vivo* precision and preliminary comparisons', OARSI 2016 world congress, March 2016.

- Arjmand, H; Nazemi, M; Burnett, WD; Kontulainen, SA; McLennan, CE2; Hazel, D; Talmo, C; Hunter, DJ; Wilson, DR; Johnston, JD,' Investigating associations between OA-related knee pain and mechanical behavior using subject-specific finite element modeling of the knee', Alberta biomedical engineering graduate conference, October 2014

- Arjmand, H; Nazemi, M; Kontulainen, SA; Milner, JS; Holdsworth, DW; McLennan, CE; Hazel, D; Talmo, C; Hunter, DJ; Wilson, DR; Johnston, JD; 'Finite element modeling of proximal tibiae: *in vivo* precision and preliminary comparisons', 23st Annual Life & Health Sciences Research Day, March 2016, University of Saskatchewan.

- Arjmand, H; Nazemi, M; Kontulainen, SA; Milner, JS; Holdsworth, DW, McLennan, CE; Hazel, D; Talmo, C; Hunter, DJ; Wilson, DR; Johnston, JD,' Investigating associations between OA-related knee pain and mechanical behavior using subject-specific finite element modeling of the knee', 22st Annual Life & Health Sciences Research Day, March 2015, University of Saskatchewan

- Arjmand, H; Burnett, WD; McLennan, CE; Hazel, D; Talmo, C; Wilson, DR; Hunter, DJ; Kontulainen, SA; Johnston, JD, 'Associations between pain and distal femoral subchondral bone mineral density in patients with osteoarthritis', 21st Annual Life & Health Sciences Research Day, March 2014, University of Saskatchewan.

- Arjmand, H; Burnett, WD; McLennan, CE; Hazel, D; Talmo, C; Wilson, DR; Hunter, DJ; Kontulainen, SA; Johnston, JD, 'Associations between pain and distal femoral subchondral bone mineral density in patients with osteoarthritis', 2nd annual research day of The Bone Imaging Group (BIG) with the assistance of Continuing Physical Therapy Education, January 2014, University of Saskatchewan.

Acknowledgement

Many people helped me during my MSc program, and without their support, this work would not have been possible.

I especially would like to thank my supervisor, Prof. J.D. Johnston for his guidance, motivations, and patience. I know that without your support, I would have given up merging the FE models in the first week! I am so grateful to you for believing in me, and your countless efforts to make our research group better and better every day.

I would also like to thank my co-supervisor, Prof. Saija Kontulainen, for her supervision, support, and encouragements. I am grateful for your many valuable inputs for promoting my research.

I would also like to thank my committee members, Prof. Walerian Szyszkowski and Prof. Mohamed Boulfiza, for their insights and helpful comments throughout committee meetings.

Many thanks go to my friends and colleagues in Mobil lab, and also Prof. Allan Dolovich, and Prof. Emily McWalter. You made my time at the U of S a delightful, and an unforgettable experience. I am grateful for your comments and suggestions during our meetings and scrums, and I have enjoyed working alongside each one of you.

Special thanks go to my mom, dad, Hamed, and Haleh for their unconditional love and endless support. Thank you for your kind words and encouragements in the days that I needed them most. I love you, and you mean the world to me.

Finally, I would like to thank my husband, Ramin, for his love, friendship, and always being there for me. Thank you for listening to all of my complaints as well as my research struggles and thoughts without ever getting tired, and for giving me that extra push whenever I am afraid to move forward.

Table of contents

List of Figures

List of Tables

List of Abbreviations, symbols and terms

Terms	Definition
Anisotropic	A material (e.g., bone) with different physical properties (e.g., material stiffness) in different directions
Apparent density	Laboratory measure of hydrated bone mass / total specimen volume (g/cm^3); synonymous with wet apparent density
Ash density	Laboratory measure of ash mass / total specimen volume (g/cm^3)
Axial	Situated in the central part of the body
Bone mineral density	Imaging measure of bone mass / total image area (DXA) or volume (QCT), referred to as BMD.
Cancellous	Type of bone tissue comprised of vertical and horizontal trabeculae which create a spongy, cellular-like tissue; typically occurs at the ends of long bones; high surface area compared to cortical bone and is, therefore, more metabolically active; synonymous with trabecular bone
Compact bone	Type of bone tissue comprised of multiple layers of compacted bone; forms the cortex or outer shell of bone; much denser, stronger and stiffer than cancellous bone; synonymous with cortical bone
Coronal	Plane that divides the body into anterior (front) and posterior (back) sections
Cortical bone	Synonymous with compact bone
Cyst	Bone void; usually present at the weight bearing region of osteoarthritic bone
Distal	Pertains to different ends of an extremity; distal end of extremity is the end situated farthest from the center of the body (e.g., distal tibia is located at ankle joint)
In situ	Latin for "in the place"; in biomechanics refers to experimentation of a largely intact structure (i.e., joint or entire bone) as opposed to (*in vitro*) experimentation of a small tissue or bone sample
In vivo	Latin for "within the living"; experimentation using a whole, living organism as opposed to partial or dead organism

Terms	Definition
Intraosseous	Within a bone
Isotropic	A material (e.g., bone) with similar physical properties (e.g., material stiffness) in all directions
Joint space narrowing	Reported change in joint space width
Joint space width	Radiographically measured distance between two articulating bones
Lateral	Situated at or extending to the side
Medial	Situated at or extending to the middle
Orthotropic material	An anisotropic material with three mutually perpendicular planes of symmetry
Osteophyte	Bony projection that forms along the periphery of joints, also known as bone spurs
Posterior	Back plane of a body (i.e., back)
Proximal	Pertains to different ends of an extremity; proximal end of extremity is the end situated nearest the center of the body (e.g., proximal tibia is located at knee joint)
Sagittal	Plane that travels from the top to the bottom of the body, dividing it into left and right portions
Sclerosis	Region of increased bone mineral density apparent on radiographs; commonly thought of as stiffening or hardening of a structure
Structural stiffness	Describes bone's response to deflection; dependent upon both material stiffness properties and physical size of the bone tissue being tested
Subchondral bone	Bone below (sub) cartilage (chondral)
Trabecular bone	Synonymous with cancellous bone
Trabeculae	Latin for "small beam"; bone tissue element in the form a small beam, strut or rod

Terms	Definition
Transverse	Plane that divides the body into superior (top) and inferior (bottom) parts; synonymous with axial plane
Valgus	Outward angulation of the distal segment of a bone or joint; at the knee synonymous with “knock-kneed”; opposite of varus
Varus	Inward angulation of the distal segment of a bone or joint; at the knee synonymous with “bow-legged”; opposite of valgus
Voxel	Volume element representing a value in three-dimensional space

Abbreviation	Description
2D	Two-dimensional
3D	Three-dimensional
95% CI	95% confidence interval
ANOVA	Analysis of variance
BMD	Bone mineral density
BV/TV	Bone volume fraction (bone volume/total volume)
CT	Computed tomography
CV%	Percentage coefficient of variation
DOF	Degree(s) of freedom
FE	Finite element
FEM	Finite element modeling
HMH	Half maximum height
HR-pQCT	High-resolution peripheral QCT imaging
HU	Houndsfield unit
K_2HPO_4	Dipotassium phosphate
KL	Kellgren-Lawrence
MRI	Magnetic resonance imaging
OA	Osteoarthritis
PF	Patellofemoral
QCT	Quantitative computed tomography
R^2	Coefficient of determination

Abbreviation	Description
RMS	Root mean square
RMSE	Root mean squared error
SD	Standard deviation
TF	Tibiofemoral

Symbol	Definition
σ	Stress (Pa)
ε	Strain
ρ	Density (kg/m^3)
ϑ	Poisson's ratio
δ	Deflection, displacement (mm)
E	Young's modulus, Modulus of elasticity (MPa)
F	Force (N)
μ	micro
E	Elastic modulus
M	Mega (e.g. MPa=Megapascal)
mm	Millimeter (length unit)
N	Newton (the unit for force)
N/mm	Newton/millimeter (the unit for structural stiffness)
Pa	Pascal (the unit for stress)
K	Structural stiffness (N/mm)
$\mu\varepsilon$	Microstrain (10^6 x strain)

1 Introduction

1.1 Overview

Osteoarthritis (OA) is a painful joint disease which affects nearly 85% of the Canadian population over 75 years of age [1]. Knee osteoarthritis is the most common form of clinically diagnosed OA [2]. Knee OA can cause extensive pain and also diminishes the quality of patients' life. There is no cure for OA; consequently, in severe cases of OA, knee replacement surgery is the only option to reduce OA-related pain and improve the quality of life.

It is widely thought that cartilage loss is the main factor in the development of OA and changes in subchondral bone are considered as a result of cartilage degradation. Because of this concept, many researchers have focused solely on the association between cartilage and OA progression; however, other studies suggest that changes in subchondral bone (bone below cartilage) in the early stages of OA play a major role in cartilage degradation, OA development, and OA-related pain [3-6]. These alterations include variable subchondral morphology and material properties as well as cyst formation (essentially voids within bone). In addition, bony osteophyte formation (bone spurs along the periphery of bone) is believed to be linked to OA-related pain and diminished functionality. Given that cartilage is aneural (lacking nerves) whereas bone is highly innervated [7, 8], bone is a potential initiatory site of pain with altered bone morphology and mechanics as the source.

Finite element (FE) modeling is a non-invasive method that has been used extensively in biomechanics to obtain mechanical properties. By using this technique, complicated structures can be studied under varying loading conditions and *in vivo* (in living) estimates of local stiffness and internal stress and strain distributions can be provided. In most FE analyses, general and simplified geometries are used, and average conclusions are drawn based on these analyses; however, to study

inter-subject variability, subject-specific FE models are needed. Quantitative computed tomography images (QCT) can be used to create subject-specific FE models (referred to as QCT-FE). This modeling technique has the potential to clarify the relation between structural and mechanical properties and OA-related pain; however, it is crucial to calculate the precision (repeatability) of FE-derived outcomes before using them for investigating, and differentiating OA and normal knees.

In this research, the first objective was to develop subject-specific FE models of OA and normal knees. The second objective was to test the precision of FE-derived estimates of stress/strain distributions, and stiffness. This precision study helps to identify precise FE parameters for future research aiming to clarify the role of bone in OA. In addition, stress/strain distributions and stiffness values were compared in OA and normal knees. This study provides the first subject-specific FE model of the knee joint with the ability to investigate the potential role of mechanical properties of subchondral bone in OA development, progression, and related pain.

1.2 Scope

Chapter 2 provides a literature review and background information on the anatomy of the knee joint, OA, and the finite element technique. In Chapter 3, research questions and objectives are outlined. Chapter 4 describes the methodology for FE modeling and calculating precision. Chapter 5 includes results of the precision study of FE outcomes and a preliminary comparison of FE-derived mechanical metrics for OA and normal knees. In Chapter 6, a discussion of study findings compared with the existing literature, main strengths and limitations of this research are presented. Chapter 7 outlines conclusions, contributions, clinical significance of this work, as well as suggested future work.

2 Background

2.1 Functional Anatomy

Three different bones form the knee joint, including the proximal tibia, the distal femur, and the patella (Figure 2-1). In addition, the fibula is located at the lateral side of the tibia and aligned parallel to the tibia. The distal femur transmits load (e.g., body weight) to the proximal tibia through the tibiofemoral (TF) articulating joint. Both the distal femur and proximal tibia consist of medial (inner part) and lateral (outer part) compartments. Typically, medial compartments transfer 2.5 times more load compared to the lateral compartments [9].

Articular cartilage, which is an aneural (without nerves) and avascular (without blood cells) tissue, covers the joint surface of the tibia, fibula, and patella. Cartilage is responsible for transferring load between two adjacent bones and is composed of an extracellular matrix (ECM), chondrocytes, collagen type-II fibers, and proteoglycans. The extracellular matrix (ECM), which is the major component of cartilage, consists mainly of water (68-85%). Chondrocytes are cartilage cells responsible for producing and preserving the ECM matrix. The Other two components are essential for mechanical properties of the cartilage; collagen type-II fibers provide shear and tension resistance, while proteoglycans contribute to the compression resistance of the cartilage. Cartilage has an incompressible behavior, and its Poisson's ratio is usually estimated from 0.45 to 0.5 [10-12].

Another tissue in the knee joint are menisci, which are two crescent-shaped wedges of fibrocartilage in the TF joint in the medial and lateral compartments (Figure 2-2). Menisci cover 59-71% of surface of the articular cartilage, and at least 50% of load is transmitted through them to the articular cartilage.

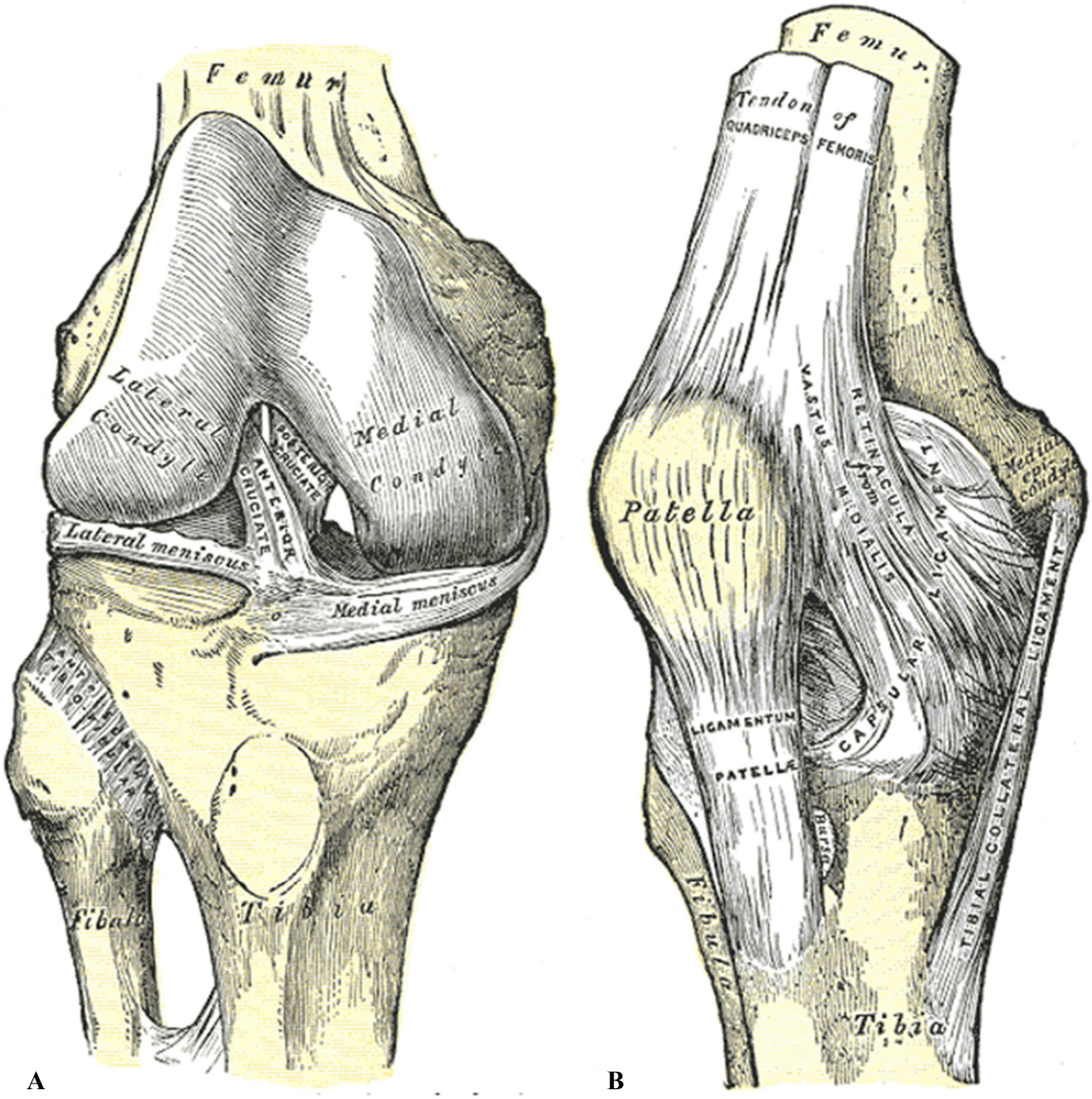

Figure 2-1- Anterior (A) and Posterior (B) view of human knee joint. Femur, tibia, fibula and patella, as well as lateral and medial compartments, are displayed. Modified from Gray's Anatomy [13].

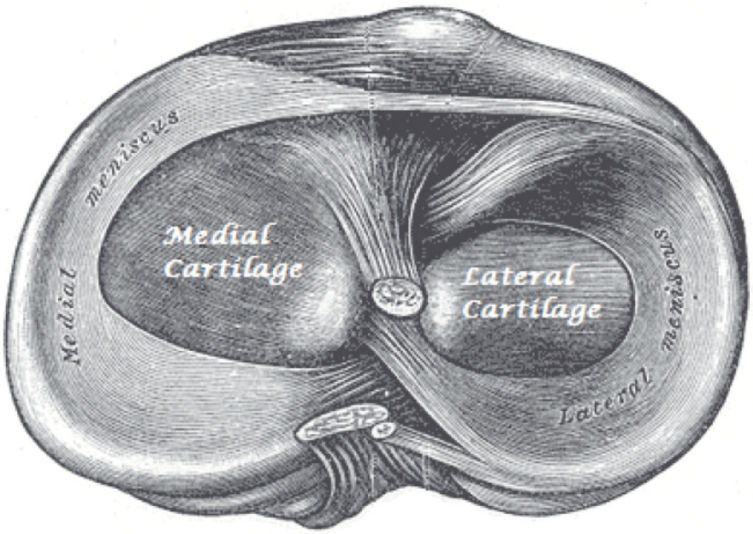

Figure 2-2- Axial view of the medial and lateral meniscus above articular cartilage of the tibial plateau. Modified from Gray's Anatomy [14].

Beneath cartilage, there are numerous bony tissues including calcified cartilage, subchondral cortical, subchondral trabecular, epiphyseal trabecular, and metaphyseal trabecular bone (Figure 2-3 and Figure 2-4). Calcified cartilage is a thin partially mineralized tissue. Subchondral cortical bone is a highly mineralized layer just beneath the calcified cartilage while subchondral trabecular bone is a spongy cancellous bone attached to the subchondral cortical bone with transitions to epiphyseal and metaphyseal trabecular bone. The term subchondral bone is used to describe the combination of subchondral cortical and trabecular bone [15]. Subchondral bone helps to stabilize the joint and cartilage as well as to transfer load between opposing articulating bones. Since cartilage is a compliant material, its health and integrity are dependent on the underlying subchondral bone [16]. As such, subchondral bone alterations might lead to cartilage damage [17, 18]. Subchondral bone is also important because it could be a source of OA-related pain as it contains a high concentration of nerve endings [8, 19]. Epiphyseal trabecular bone is

beneath the subchondral trabecular bone at the proximal epiphysis. Metaphyseal trabecular is located under the epiphyseal trabecular bone at the proximal metaphysis.

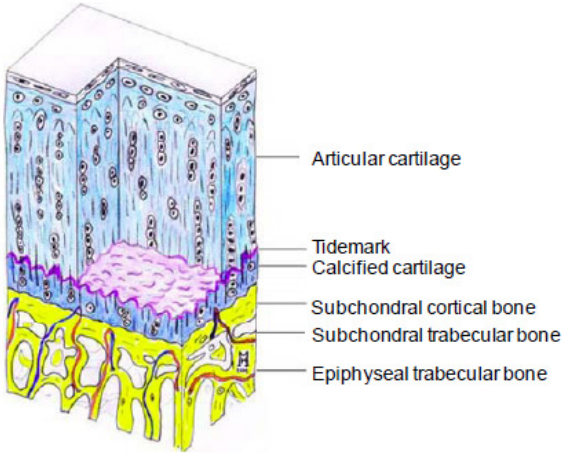

Figure 2-3- Different layers of cartilage and subchondral bone including articular cartilage, subchondral cortical, subchondral trabecular and epiphyseal trabecular bone [20], Modified from Imhof et al. [21] and Madry et al. [22].

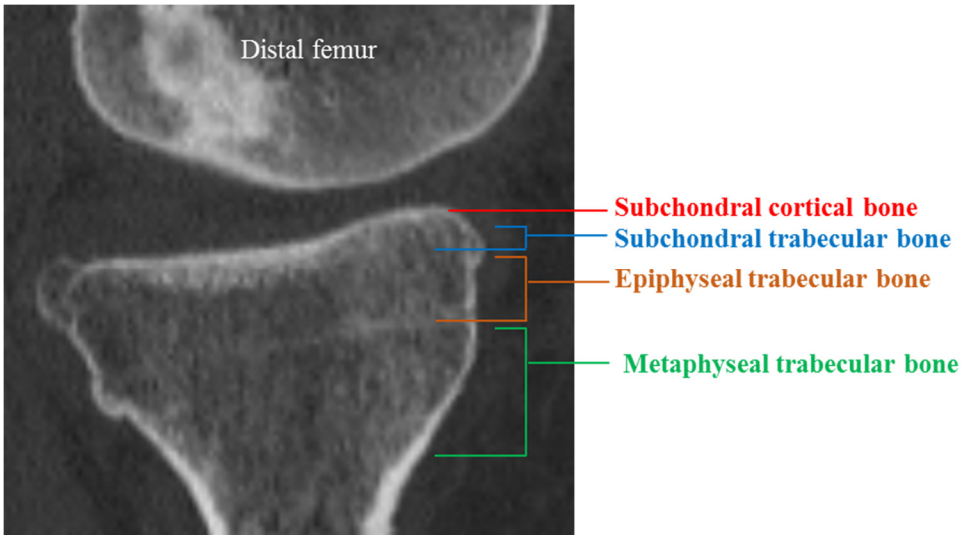

Figure 2-4- Different layers of bone including subchondral cortical, subchondral trabecular, epiphyseal trabecular, and metaphyseal trabecular are shown in a sagittal section of a CT image of the proximal tibia.

2.2 Osteoarthritis Characteristics

Some common clinical symptoms of OA include joint pain, swelling, joint stiffness, and limited range of motion; with pain being the main symptom of OA. However, the source of OA-related pain is largely unknown [23-27]. Although OA is generally considered to be a disease of cartilage, it also affects other tissues including subchondral bone [28, 29]. OA alters morphology and biomechanical properties of both bone and cartilage. Biomechanical alterations include lower tensile and shear strength along with lower compressive stiffness of cartilage, and altered mechanical stiffness of the subchondral bone [30]. Morphological alterations include cartilage loss in load bearing areas; larger subchondral bone thickness, volume, and density; subchondral cyst formation within the trabecular bone; and osteophyte formation along the joint periphery [31]. Figure 2-5 shows an OA knee with a narrowed joint space and bone on bone contact on the medial part.

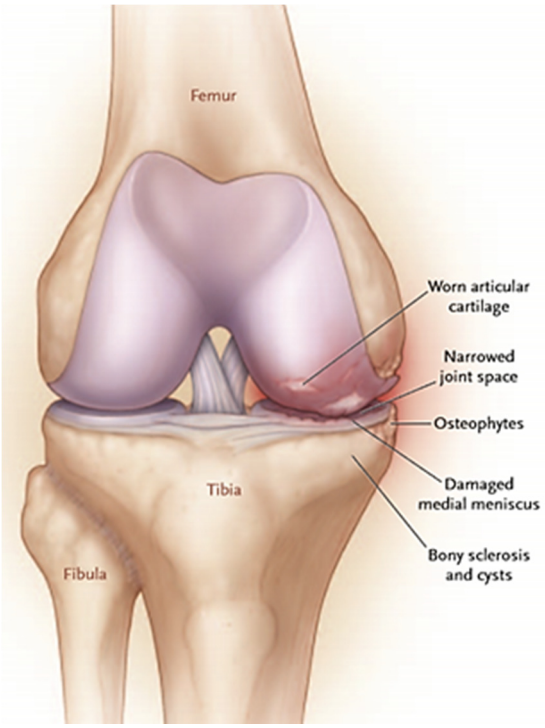

Figure 2-5- Illustration of medial OA, with medial plateau having bone-on-bone contact [3].

2.2.1 Osteophytes

Osteophyte formation along the periphery of the bone is one of the main radiographic markers of OA (Figure 2-6). It is unclear, however, what mechanical role osteophytes have in OA. Osteophyte formation might be due to malalignment and joint laxity associated with OA. This active bony adaptation creates a larger joint surface, and could contribute to normalizing loading in joint. Various studies reported positive association between presence of osteophyte and OA-related pain, particularly in mid-stage OA [25, 32-34]. Though, a previous study in our research group showed that they did not considerably change the overall stiffness of the proximal tibia [35].

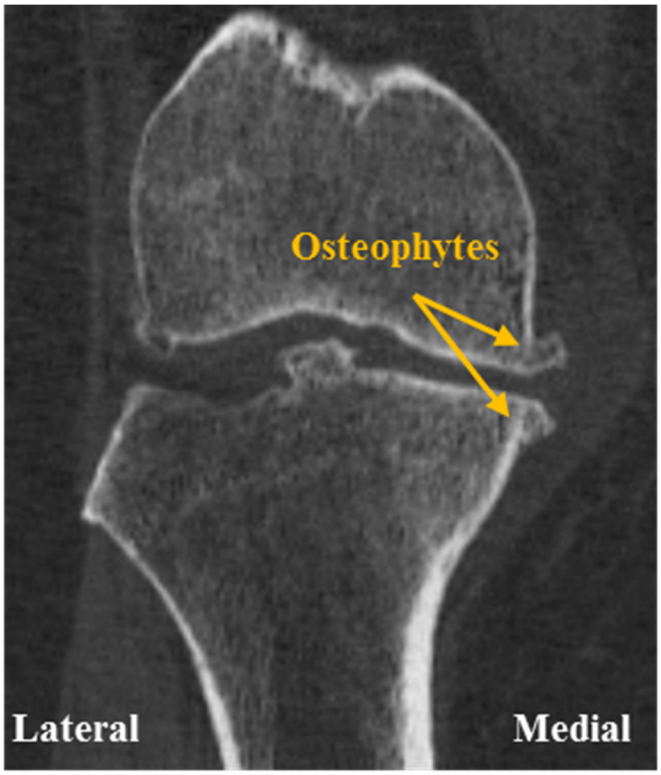

Figure 2-6- Coronal section of a CT image showing presence of medial osteophyte at the distal femur and proximal tibia.

2.2.2 Cysts

Cysts are one of the most common features of OA and they are present in the weight bearing area of the joint (Figure 2-7). Cysts are essentially voids within bone and act as stress raisers in the subchondral bone [36]. They could appear in various sizes and different shapes including ellipsoid, sphere, and pyriform. There are two theories for the development of cyst [36-38]: one theory is based on bone resorption due to the impact of the two opposing bone in the joint [37]; whereas in the other theory, increased pressure due to intrusion of synovial fluid in the subchondral bone is thought to cause cyst development [39]. The presence of a subchondral cyst in bone induces a mechanical stress peak in the subchondral bone region, which might contribute to OA-related pain [36].

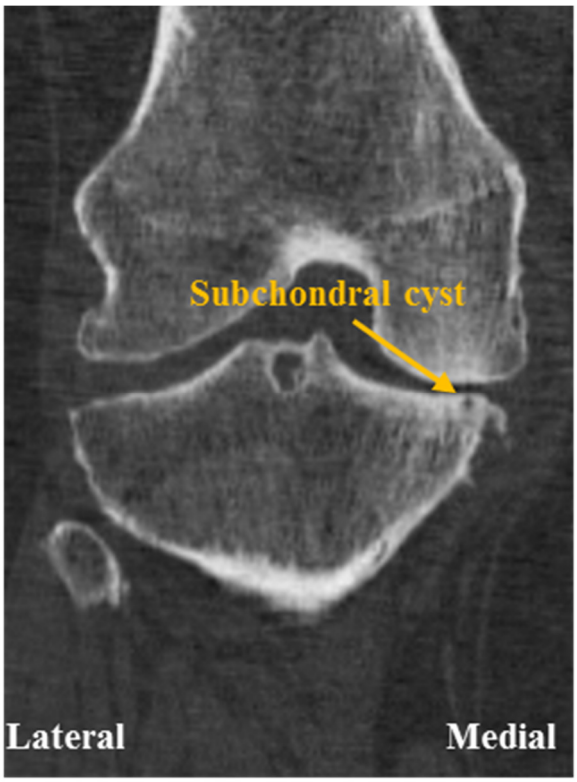

Figure 2-7- Coronal section of a CT image showing a medial cyst in the subchondral bone of the proximal tibia.

2.2.3 Malalignment and OA

In a perfectly aligned knee, the load bearing line is a straight line passing through hip, knee and ankle joint. When varus (bow-legged) or valgus (knocked-knee) happens, loading axis is shifted either to the inside (varus) or outside (valgus) of the knee; therefore, loading increases on medial (varus) or lateral (valgus) compartments. Studies show that there is a link between varus and valgus malalignment and knee OA, and its progression [40-44]. Figure 2-8 shows a knee joint with varus alignment.

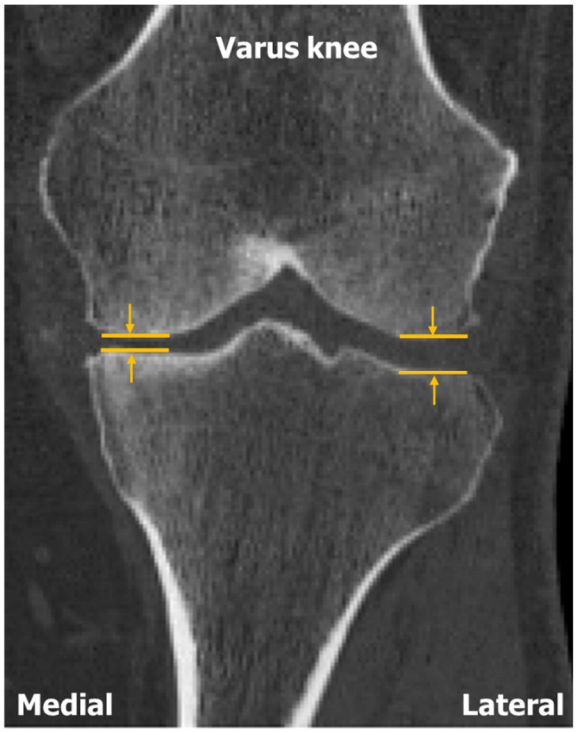

Figure 2-8- Coronal reconstruction of CT image of OA knee with varus (bow-legged) malalignment. In a varus knee, the joint space is more in the lateral side.

2.2.4 Alteration in Bone Densities

Altered bone mineral density (BMD) is a common marker of OA. Studies report that while higher BMD is common in OA [45-48], loss of BMD appears to be closely related to pain [49, 50].

Recently, our research group reported relationships between pain and both patellar and proximal tibial subchondral BMD [49-51]. The results indicated that low medial BMD was associated with pain [49, 50].

Although these findings suggest an association between subchondral bone density and OA progression and related pain, rationale regarding this association is unclear. The main hypothesis is that observed BMD differences are associated with mechanical behavior (e.g., altered stiffness and/or loading patterns) which contribute to OA-related pain. Radiography can only identify BMD changes of greater than 30 percent [52]. Finite element modeling though may be able to capture the effects of small BMD changes (e.g., 10%) on overall mechanical behavior or stress/strain distribution.

2.3 Finite Element Modeling

FE modeling has been used to investigate the effect of OA-related morphological and mechanical property alterations on overall structural behavior, typically with idealized models. These studies tested whether altered subchondral morphology and mechanical properties, cyst formation, and alignment changed stress/strain distributions and structural stiffness of bone.

2.3.1 Stiffness Effects

Previous research has shown that OA bone has a higher thickness and density [5, 16, 53-57]. This is the origin of the theory that states that a stiffer subchondral bone could change loading and stress distributions in the joint, and lead to OA [56, 58]. In a study by Brown, a simplified plane-strain FE model was used to explore the effect of localized subchondral stiffening on mechanical stress in bone and cartilage. This FE model was based on an animal model (sheep), and localized stiffening was achieved by implanting metal cylinder beneath the subchondral bone (Figure 2-9). The FE model consisted of trabecular bone with a metal implant, the subchondral plate, the

articular cartilage, and an indentor for applying load. Linear contact-impact elements were used to model contact between the indentor and cartilage. The sensitivity of this FE model to material property inputs was investigated by varying the elastic modulus (E) of the cartilage, subchondral bone, and trabecular bone over a range of values. Results of this study indicated that local stiffening of subchondral bone increased stress in overlying cartilage by nearly 50% [6]. This study supports the theory that changes in elastic modulus of the subchondral bone can alter stress distribution in the joint, potentially lead to OA. Limitations of this study though included: (1) an oversimplified geometry; and (2) an indentor for applying the load, which fails to mimic actual loading condition in the joint.

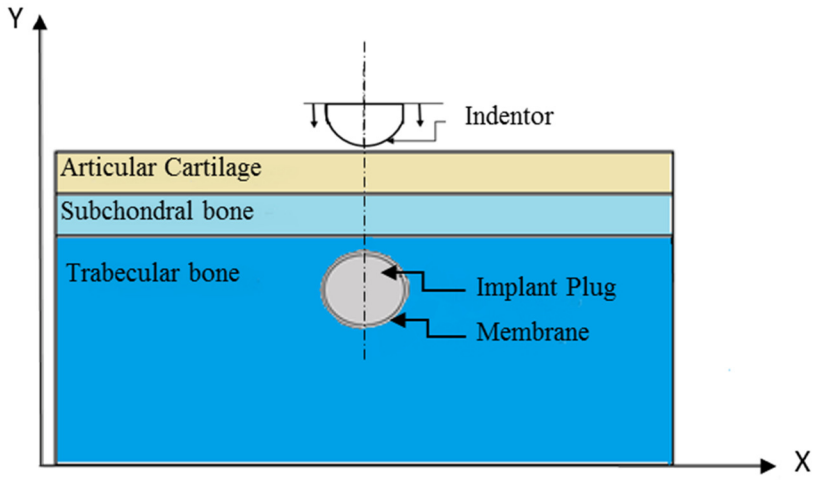

Figure 2-9- A simplified FE model of the knee joint. Subchondral bone stiffening was modeled using a cylindrical metal implant. Modified from Brown et al. [6].

In a recent study by our research group, Amini et al. developed a 3D axisymmetrical, parametric FE model of the tibia to study the effects of simulated bone changes (i.e., adding osteophytes, and changing thickness and elastic modulus of the different layers of the bone) on the local stiffness of subchondral bone [35]. The tibia model was based upon a representation sample

of 16 cadaver tibia CT images. The lateral compartment of a specimen with closest total volume and medial and lateral areas to the average values was used to create an axisymmetric FE model. To develop the parametric FE model, different layers of the bone tissue in the tibia including subchondral cortical, subchondral trabecular, and epiphyseal trabecular bone were segmented (outlined) in the CT image using image processing software (ANALYZE). To examine the effects of osteophytes on stiffness and load distribution, osteophytes with different diameters were simulated in the FE model. Linear transversely isotropic material properties were used in the FE models, and heterogeneity of the trabecular bone was modeled with assigning 16 (14 in trabecular bone, 2 in cortical bone) different elastic moduli to this region (Figure 2-10).

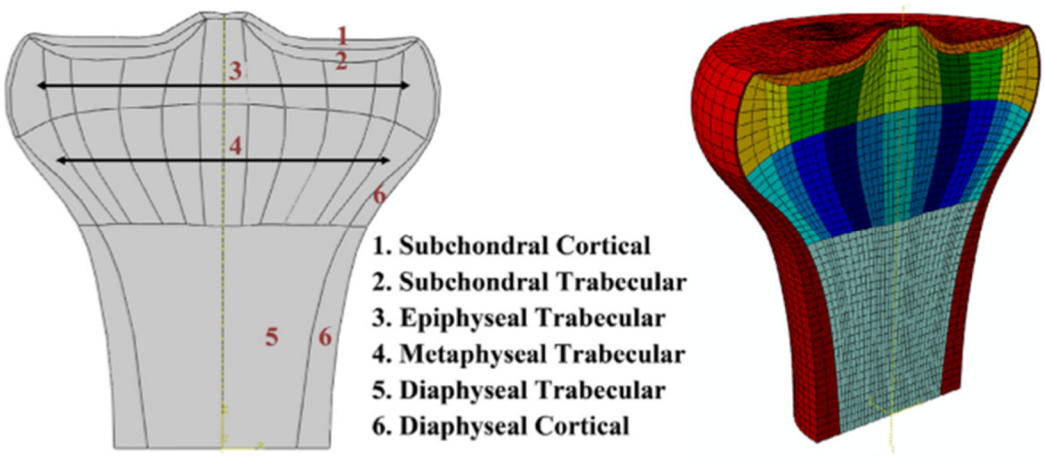

Figure 2-10- Sixteen different material properties were assigned to the proximal tibia. Each color shows different elastic modulus in the picture [59].

An elliptical Gaussian pressure distribution representing a 750 N (loading in a single-leg stance) was applied to the lateral compartment. Boundary conditions were also applied at the most distal nodes and nodes at the symmetry axis. Local stiffness was defined by dividing the applied load on the average vertical displacement in the loading region. Results of this study showed that subchondral bone stiffness was most affected by the elastic modulus of epiphyseal trabecular bone

[59]. This parametric study gives insight into the role of trabecular bone on the stiffness of the subchondral bone, and allowed the authors to easily change different parameters in the FE model to study their effects on structural stiffness of the proximal tibia. The limitation of this study though included: (1) using simplified axisymmetric geometry; (2) simplified material properties; and (3) simplified loading condition. The overly simplified geometry failed to account for the actual alterations in the bone caused by OA. It is also likely that using transitioning homogeneous material properties had an effect on the calculated FE-based structural stiffness in this study.

2.3.2 Cyst Effects

FE modeling has been also used to examine the effects of cysts on stress distribution in bone. In a study by Durr et al., an axisymmetric FE model was developed to test the hypothesis that subchondral cysts in the osteoarthritic hip joint were caused by micro-fractures in bone structure due to the loss of the cartilage and increased subchondral bone stress [37]. The FE model was comprised of the acetabulum, cartilage, and femoral head. Linear, homogeneous and isotropic material properties were assigned when modeling the cortical, trabecular bone, and cartilage. Effects of different cartilage defects and thinned cartilage on mechanical stress were investigated using FE modeling. A high peak of von-Mises stress (an indicator of possible micro-fractures in bone) was observed when creating defects in cartilage. Authors concluded that subchondral bone cysts in the osteoarthritic hip joint could be a result of bone resorption (breakdown of bone) due to excessive mechanical stress in bone. Limitations of this study, which could have affected conclusions, included: (1) simplified axisymmetric geometry; (2) introduced defects in the cartilage; and (3) simplified uniform isotropic material properties.

In another study, McErlain et al. investigated the effect of cysts on stress distribution in the proximal tibia using subject-specific FE modeling [36]. Computed tomography (CT) images

of 20 participants with early-stage knee OA were utilized in this study. First, the 3D subject-specific geometries of the knee joints were segmented from CT images. The segmented bones were then converted to FE models. Subsequently, CT-based bone densities were then converted to elastic moduli of the elements of bone using published density-modulus relationships [discussed more in section 2.3.5]. This approach incorporated bone heterogeneity into the models. Radiation is not absorbed by cartilage; thus, cartilage does not appear in CT images, and CT images are unable to characterize cartilage. As such, a homogeneous incompressible isotropic material (E=10 MPa, ν=0.495) was used to model cartilage and soft tissue in the knee joint and to mimic load transfer between femur and tibia (Figure 2-11).

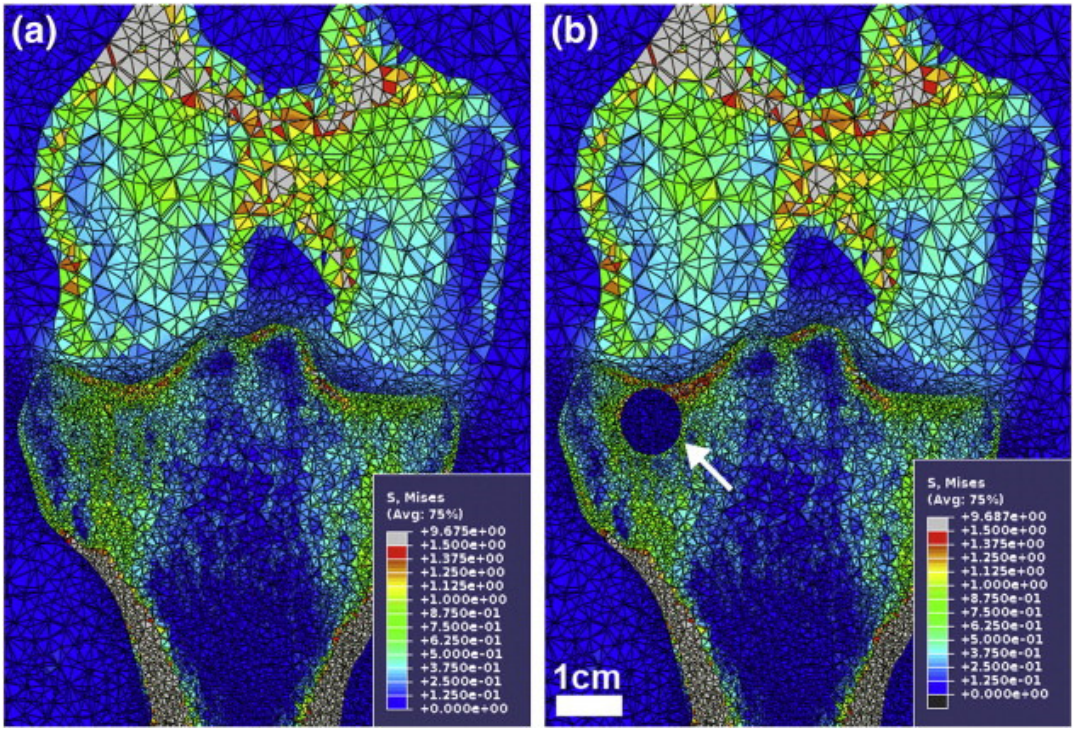

Figure 2-11- Comparison of von-Mises stress patterns in proximal tibia with and without subchondral cyst. An isotropic homogeneous material is used to model the cartilage and the soft tissue in the knee joint (shown with blue color outside of the proximal tibia and distal femur in the picture). From McErlain et al. [36].

Since participants in this study were in the early stages of OA, there was no significant cyst visible in the CT images. To overcome this limitation, authors manually introduced a virtual subchondral bone cyst (a hollow sphere which essentially acted as a stress raiser) in their model. These virtual cysts were created inside or adjacent to the subchondral bone of the distal femur or the proximal tibia without breaching the bone surface. The weight of an average person (750N) was applied to the end section of the bone without the cyst to simulate single leg stance. Nodes at the cortical shell in this section were allowed to move only vertically whereas nodes of the bone with the simulated cyst were constrained in all directions. Von-Mises stress around the cyst was obtained and compared to the stress values in duplicate models without the synthetic cysts. Higher stress in the vicinity of the cyst compared to the cyst free areas, as well as a positive correlation between the diameter of cyst and stress, were the findings of this study [36]. One of the main limitation of this study was using spheres with different diameters to simulate cysts in the subchondral region whereas subchondral cysts are hardly a perfect sphere, and they usually have a shell of high BMD around them (Figure 2-12). Also, to investigate the effect of cyst diameter on developed stress, FE-based von-Mises stress of the subchondral bone of 20 patients were compared. For each patient a different size of cyst in either tibia or femur was introduced in the FE model. In this approach, not only the diameter of cysts could affect the maximum stress values, but also location of the introduced cysts (whether it is on tibia or femur), and different bone characteristics of each patient (e.g., geometry, stiffness) could also change the observed peak von-Mises stress. This questionable comparison method might result in a misleading conclusion. Moreover, this study lacked information regarding precision or validation, which is another limitation of this research.

Figure 2-12- Medial subchondral cysts, with a shell of high BMD around each one of them, are shown in a coronal section of the proximal tibia and the distal femur.

2.3.3 Alignment Effects

Previous research indicates that malalignment (varus or valgus) alters loading distribution in the knee joint, and this abnormal loading condition could lead to OA [60]. Since bone can adjust to the different loading levels due to its remodeling and resorption characteristics, it is believed that altered loading could also alter BMD distribution of subchondral bone. A 3D FE model of a proximal tibia, combined with bone remodeling theory, was developed to investigate the relationship between valgus deformity and BMD [44]. This study simulated BMD changes in a 3D model of the proximal tibia for normal and 6° valgus knees. The loading distribution, including contact and ligament forces, were obtained from gait analysis (Figure 2-13). It was shown that valgus malalignment could change BMD distribution in subchondral bone, potentially leading to OA. Limitation of this research included: (1) only gait analysis of a normal knee was used in the study; (2) a different load bearing ratio between medial and lateral compartments was used to

model valgus deformity in the FE model of a normal proximal tibia instead of true malalignment between the opposing tibia and femur.

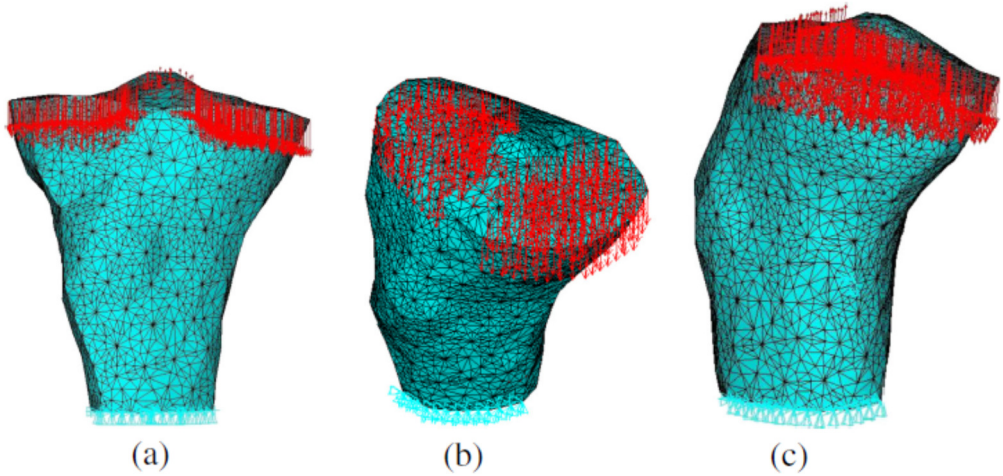

Figure 2-13- 3D finite element modeling of the proximal tibia, (a) front view, (b) top view, (c) right view [44].

2.3.4 Pain Effects

One of the probable causes for OA-related pain might be higher mechanical stress or strain in the subchondral bone, causing stimulation of nerves in the bone; however, there is no study in the literature supporting this theory. In an *in vivo* patella study, Farrokhi et al. analyzed stress patterns in the patellofemoral (PF) joint with nonlinear FE modeling [11]. The data from 20 female patients (10 with PF pain, and 10 without pain) were used for this study. Subject-specific joint geometry, kinematics and muscle forces in the FE model were obtained from magnetic resonance (MR) images and biomechanical tests. Bones were modeled as rigid bodies and an isotropic homogeneous material property was used for modeling cartilage (E=4 MPa, ν=0.47). In the FE model, hydrostatic pressure and octahedral shear stress as the two components of stress in cartilage were studied, and two-way analysis of variance (ANOVA) was used to analyze results. The study revealed that patients with more PF pain had higher PF cartilage stress (both hydrostatic pressure and octahedral shear stress). Authors stated that hydrostatic pressure could stimulate nerves at the

subchondral bone to cause pain, which supports the prospect that pain could be a result of aberrant joint loading [61]. This study highlights the association between mechanical properties (i.e. stress) of the joint and pain, with the main focus being on cartilage; however, using flexible bones instead of rigid bodies, the mechanical behavior could be studied directly in subchondral bone as a potential initiatory site of pain.

2.3.5 Subject-Specific Finite Element Modeling

Subject-specific FE modeling using CT images is a powerful technique to investigate bone behavior *in vivo*. Generally, the geometry of the bony tissues are obtained using segmentation of CT images and image-based densities are converted to elastic moduli using published density-modulus relationships (commonly referred as E-BMD relationships). Table 2-1 shows some of the common equations available in the literature for elastic modulus and bone density. Various forms of bone densities are used in these relationships; some of the most popular types of reporting bone density in the literature and their definitions are gathered in Table 2-2. These density measurements could also be converted to each other using known relationships between them (Table 2-3).

Table 2-1- Common relationships between elastic modulus of bone and bone densities. Modified from Helgason et al. [62]. Various forms of bone densities in these relationships are defined in Table 2-2. $\dot{\varepsilon}$ is the strain rate to which bone is subjected.

Study	Site	Type of bone	Density	ρ - range (g/cm^3)	E (GPa)
Carter and Hayes [63]	Pooled	Cortical and trabecular	ρ_{app}	0.07-2.0	$E = 3.79\dot{\varepsilon}^{0.06}\rho_{app}^{3}$
Lotz [64]	Human Femoral neck	Trabecular	ρ_{app}	0.18-0.95	$E = 1.31\rho_{app}^{1.40}$
Lotz [65]	Human Femoral metaphysis	Cortical	ρ_{app}	1.2-1.85	$E = -13.43 + 14.261\rho_{app}$
Snyder and Schneider [66]	Human tibial diaphysis	Cortical	ρ_{app}	1.748-1.952	$E = 3.891\rho_{app}^{2.39}$
Hodgskinson and Currey [67]	Pooled	Trabecular	ρ_{dry}	0.094-1.111	$E = 3.980\rho_{dry}^{1.78}$
Linde [68]	Human proximal tibia	Trabecular	ρ_{app}	0.273	$E = 4.778\rho_{app}^{1.99}$
Anderson [69]	Human proximal tibia	Trabecular	ρ_{dry}	0.14-0.48	$E = 3.890\rho_{dry}^{2.0}$
Keller [70]	Human femur	Cortical and trabecular	ρ_{ash}	0.092-1.221	$E = 10.5\rho_{ash}^{2.29}$
Keller [70]	Pooled	Cortical and trabecular	ρ_{ash}	0.028-1.221	$E = 10.5\rho_{ash}^{2.57}$
Keyak [71]	Human proximal tibia	Trabecular	ρ_{ash}	0.06-0.27	$E = 33.9\rho_{ash}^{2.20}$
Goulet [72]	Pooled	Trabecular	BV/TV	0.06-0.36	$E = 6.310(BV/TV)^{2.10}$
Li and Aspden [55]	Human femoral head	Trabecular	ρ_{app}	0.14-1.4	$E = 0.573\rho_{app} - 0.0094$
Ciarelli [73]	Human proximal femur	Trabecular	BV/TV	0.15-0.40	$E = 7.541(BV/TV) - 0.637$
Morgan [74]	Human proximal tibia	Trabecular	ρ_{app}	0.09-0.41	$E = 15.52\rho_{app}^{1.93}$
Morgan [74]	Human femoral neck	Trabecular	ρ_{app}	0.26-0.75	$E = 6.850\rho_{app}^{1.49}$
Morgan [74]	Pooled	Trabecular	ρ_{app}	0.09-0.75	$E = 8.920\rho_{app}^{1.83}$
Kaneko [75]	Human distal femur	Trabecular	ρ_{ash}	0.102-0.331	$E = 10.88\rho_{ash}^{1.61}$

Table 2-2- Bone density definition, Modified from Helgason et al. [62].

$\rho_{real}\left(g/cm^3\right) = \text{Real density} = \frac{\text{hydrated tissue mass}}{\text{bone tissue volume}}$	[76]
$\rho_{app}\left(g/cm^3\right) = \text{Apparent density} = \frac{\text{hydrated tissue mass}}{\text{total speciman volume}}$	[76]
$\rho_{wet}\left(g/cm^3\right) = \text{Apparent wet density} = \frac{\text{hydrated tissue mass}}{\text{total speciman volume}}$	[71]
$\rho_{dry}\left(g/cm^3\right) = \text{Apparent dry density} = \frac{\text{dry tissue mass}}{\text{total speciman volume}}$	[70]
$\rho_{ash}\left(g/cm^3\right) = \text{Ash density} = \frac{\text{ash mass}}{\text{total speciman volume}}$	[76]
$\rho_{act}\left(g/cm^3\right) = \text{Actual density} = \frac{\text{total speciman mass*}}{\text{total speciman volume}}$	[77]
$\text{Porosity} = 1 - \frac{\text{apparent density}}{\text{real density}}$	[77]
$\frac{BV}{TV} = \text{Bone volume fraction} = \frac{\text{Bone tissue volume}}{\text{total speciman volume}} = \frac{\text{apparent density}}{\text{real density}}$	[78]

* *The specimen mass including marrow*

Table 2-3- relationships between different measurements of bone densities, Modified from Nazemi et al. [79].

$\rho_{ash} = 0.55\rho_{app}$	[62]
$\rho_{ash} = 0.597\,\rho_{dry}$	[80]
$\rho_{real} = 1.8\ g/cm^3$	[63]
$\rho_{app} = \rho_{real} \times BV/TV$	[62]
$BMD = 0.904\rho_{ash} - 0.0321$	[80]
$\rho_{ash} = 1.06BMD + 0.0389$	[80]

The selected E-BMD relationship is very important for developing an accurate FE model [81]. In a study by Austman et al., authors used six different E-BMD relationships for FE modeling of the ulna, and the error reported in this study for predicting surface strain ranged from 15.3 % to 92.4%. In this work and in related references, it was observed that using anatomic and species-specific E-BMD relationships were crucial for obtaining accurate FE results [74, 82]. In a recent subject-specific FE modeling study, Nazemi et al. compared nine different E-BMD relationships for modeling the proximal tibia; two of these equations were cortical-specific and seven of them were trabecular-specific equations [79]. This study compared local subchondral bone stiffness obtained from mechanical macro-indentation tests with the FE-based stiffness values (macro-indentation tests measure structural stiffness at the subchondral surface using a flat cylindrical indentor, and give a close estimate of *in vivo* stiffness measures [83]). Nine lateral and four medial compartments of 11 fresh frozen cadaveric proximal tibial samples were used in the experimental setup and CT images of them were acquired. CT grayscale values were converted to BMD using a QCT phantom (Figure 2-14). Macro-indentation tests were performed at 47 locations from 13 samples. Experimental local structural stiffness was defined by the slope of the most linear part of the force-displacement curve of the macro-indentation tests. Using QCT images and E-BMD relationships for the proximal tibia, FE models were developed. E-BMD relationships employed in this study were either specific to the tibia or pooled from various anatomical sites including proximal tibia. Material properties were mapped using only trabecular-specific equations, and also trabecular-specific and cortical-specific equations together. Authors concluded that combination of the equations proposed by Goulet et al. for tibial trabecular [72], and Snyder and Schneider (R^2=0.75, RMSE=850 N/mm) [66] or Rho et al. (R^2=0.77, RMSE=1260 N/mm) [84] for tibial cortical bone were best suited for subject-specific FE modeling of the proximal tibia. Though,

when using a single E-BMD equation with Goulet et al. [72] stiffness predictions were similar (R^2=0.7, RMSE=728 N/mm). This was the first validated FE study for the local structural stiffness at the subchondral surface. Using E-BMD relationships suggested in this study, accurate and precise FE models could be developed to investigate the effects of altered morphological and mechanical properties of subchondral bone, as well as cysts and malalignment, on mechanical behavior and load transmission in the knee joint, and also study their links with pain.

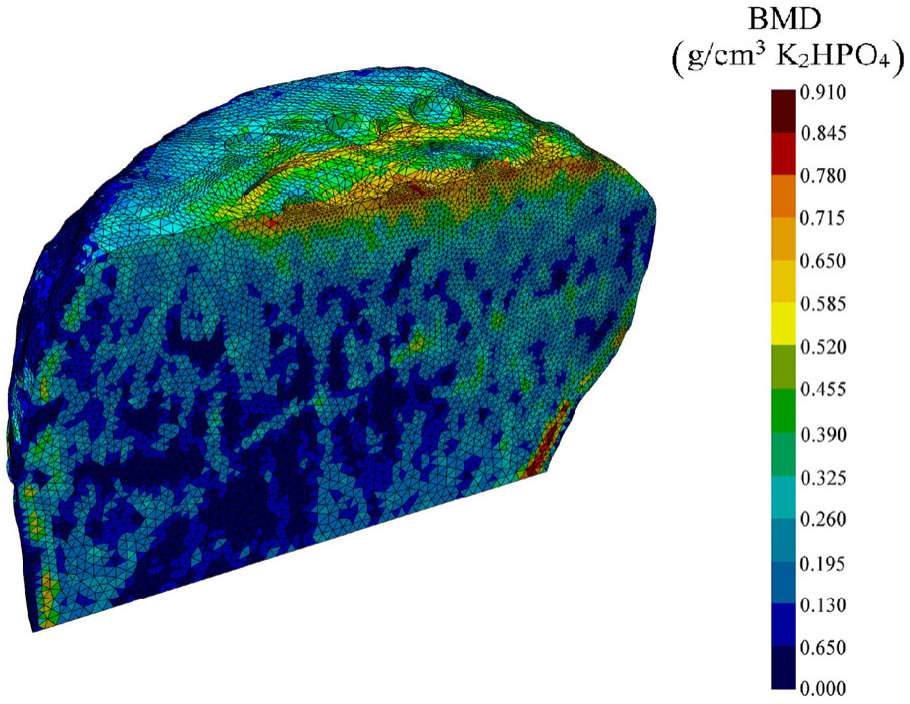

Figure 2-14- BMD distribution in a sagittal section of a proximal tibia. Indentaion sites are shown with the cylindrical walls on the subchondral surface [79].

2.4 Summary

Although previous studies highlight the potential role of bone in OA initiation and development, most research to date has been simulation-based. In these studies, simplified geometry, loading, and material properties as well as synthetic defects in the bone were used to study OA bone and

associated altered mechanical environment .To our knowledge, there is no study in the literature examining the combined effects of the individual alterations (i.e., BMD alterations, alignment, presence of cyst, etc.) on mechanical behavior, load transmission, and stress/strain distributions, *in vivo*. Current theories for the role of subchondral bone in OA are obtained from animal or *ex vivo* cadaveric studies. Since animal studies may not apply to human OA, and the clinical status or pain symptoms are often unknown in cadaveric studies, accurate *in vivo* models are needed. Subject-specific FE modeling has potential to clarify the role of subchondral bone in OA while assessing various mechanical properties of the bone (which cannot be measured otherwise), and studying them in OA and normal knees. However, before using this technique to study OA and normal knees, we need to determine the precision error of FE-derived mechanical properties.

2.5 Research Questions

The overall goal of this study was to develop a precise FE model of the knee to investigate the role of bone in OA. This research aims to answer the following research questions:

1- Can subject-specific FE modeling be used to characterize structural stiffness and stress/strain distributions in OA and normal knees?

2- How precise are FE-based outcomes of proximal tibia stiffness and stress/strain distributions, *in vivo*?

3- Do FE-based outcomes of stiffness and stress/strain distributions differ between OA and normal knees?

2.6 Research Objectives

To address these research questions, the specific objectives to be achieved include:

1- Develop a subject-specific FE modeling methodology for the OA and normal knee joints.

2- Determine the *in vivo* precision of proximal tibia stiffness and stress/strain distributions offered using FE.

3- Determine whether FE-derived metrics discriminate normal and OA knees.

3 Methodology

3.1 Study Participants

Fourteen participants (3 men, 11 women) aged 23 to 71 (mean ±standard deviation (SD): 49.9 ± 11.9 years) were recruited for this study. Informed consent from all participants and institutional review board (IRB) approval were obtained prior to the study initiation.

3.2 OA Assessment

Some participants were suffering from diagnosed knee OA or undiagnosed knee pain. If the participants had knee pain, the most painful knee was selected for imaging; otherwise, a random selection of left or right knee was scanned. OA assessment was performed using a modified Kellgren–Lawrence (KL) OA severity scoring system by an orthopaedic surgeon (Dr. Bassam Masri) [85]. The modified KL OA scoring system was mostly based on presence of osteophytes and sclerosis in the images while joint space narrowing was considered in a lower degree. The specific OA severity classification was as follow:

0 Normal, no osteophytes

1 Possible osteophyte lipping

2 Definite osteophytes, possible joint space narrowing

3 Moderate or multiple osteophytes, definite joint space narrowing, some sclerosis and possible bony deformity

4 Large osteophytes, marked joint space narrowing, severe sclerosis, and definite bony deformity

Seven of 14 knees showed evidence of osteophyte and sclerosis. Therefore, they were classified as OA (1M, 6F; 52.4 ± 8.7 years; 1 with KL=1-2; 3 with KL=2; 2 with KL=3; 1 with KL=4). In general, early OA is defined as KL=1-2 while late OA is KL=3-4. In remaining seven

knees, OA severity score was zero, and no evidence of osteophyte and sclerosis was present in the images. These knees were classified as normal (KL=0; 47.3 ± 14.8 years).

3.3 CT Imaging

3.3.1 QCT Acquisition

The knee of interest for each participant was imaged via single-energy QCT using a clinical CT scanner (Lightspeed 4-slice, General Electric, Milwaukee, WI, USA). Scanning was performed in the supine position of participants while the knee of interest was centered within the CT gantry. A solid QCT reference spine phantom (Model 3T; Mindways Software Inc, Austin, TX, USA) was included in the images in order to convert grayscale CT Hounsfield units (HU) to equivalent apparent volumetric BMD (mg/cm^3 K_2HPO_4) (Figure 3-1). Scanned image volumes contained the distal femur, patella, proximal tibia, and fibula, though image volumes were cropped to exclude the patella for this analysis. CT scanning parameters included: 120 kVp tube voltage, 150 mAs current-time product, axial scanning plane, 0.625 mm isotropic voxel size (0.625 mm slice thickness, 0.625 x 0.625 mm in-plane pixel size), ~240 slices, ~90 s scan time. Participants were scanned three times over two consecutive days, with repositioning between repeated scan, and a maximum of two scans in each day. Edge enhancement and post-processing was done using a standard bone reconstruction kernel (BONE).

3.3.2 BMD Conversion

A linear regression equation ($R^2 > 0.99$) was derived from the mean CT grayscale intensities (Hounsfield units, HU) and known reference phantom densities. The regression equation was used to convert HU to equivalent volumetric BMD, using a custom code in MATLAB.

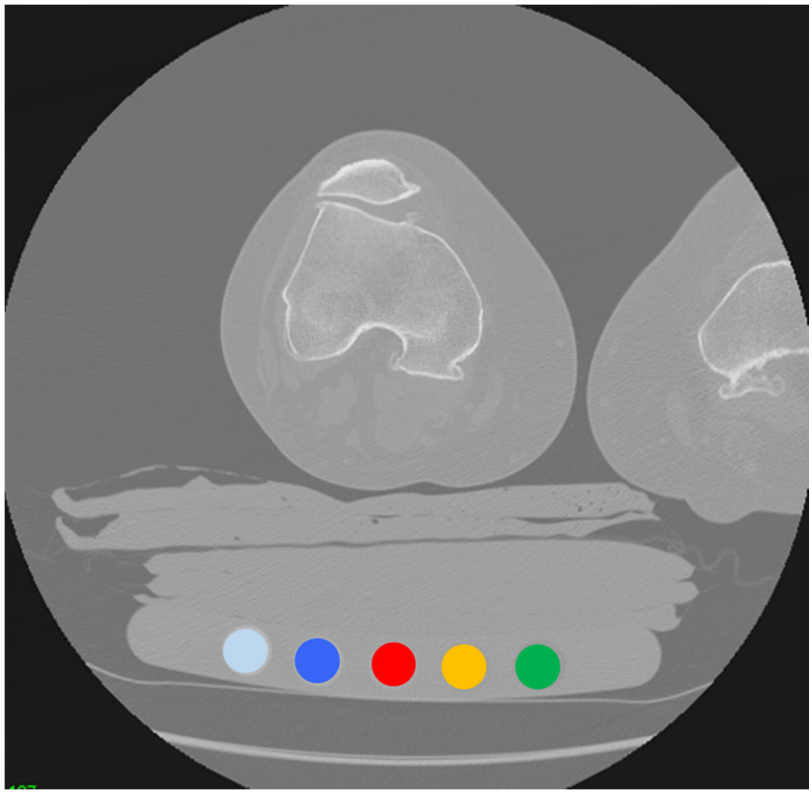

Figure 3-1- Converting CT grayscale units to BMD using a reference phantom.

3.3.3 CT Image Analysis

3.3.3.1 Image Segmentation

The proximal tibia, distal femur, and fibula were segmented from the surrounding soft tissue in the QCT images using commercial image processing software (ANALYZE) (Figure 3-2- A, B). A subject-specific bone threshold, obtained using the half maximum height (HMH) technique, was used for segmenting each image [86, 87]. In order to employ this technique, a relatively flat and small region in both medial and lateral compartments of the tibia was selected. This region included approximately half joint space and half subchondral cortical bone. In the HMH method, the density of a voxel with 50% cortical bone and 50% joint space is used as the minimum threshold for segmenting subchondral bone.

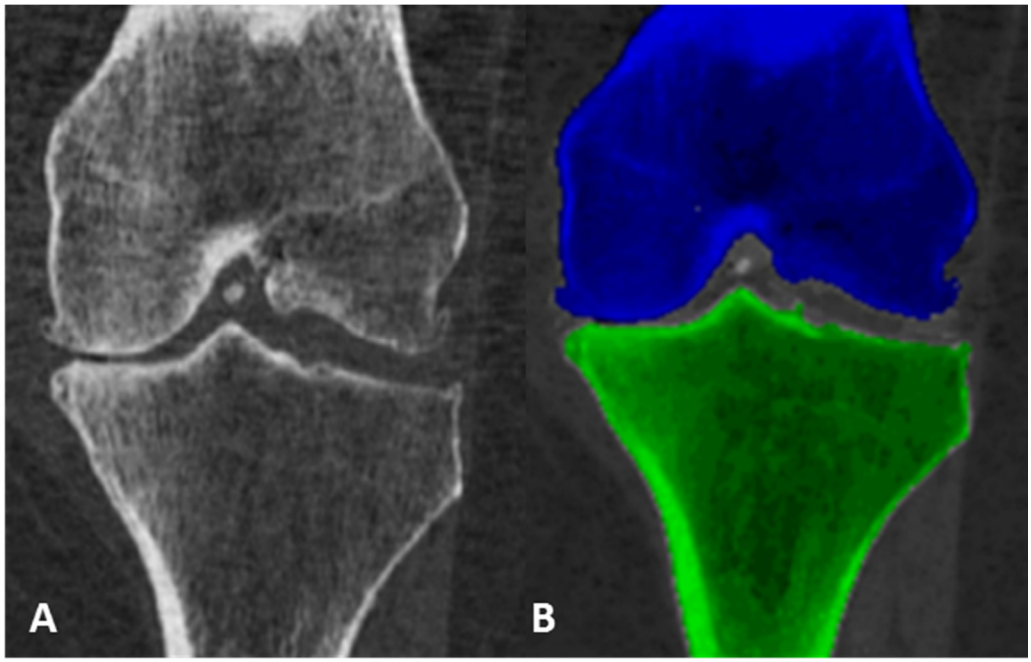

Figure 3-2- (A) CT image of the knee. (B) Segmented bones of the knee. Image shows femur (blue) and tibia (green) in coronal reconstruction of CT image.

Segmentation was done separately for the distal femur, the proximal tibia, and the fibula on series of 2D CT images. In the ANALYZE software, boundaries for the segmented region was defined by placing a 2D seed with a minimum threshold of HMH value of the bone of interest in the subchondral cortical bone. To ensure that the entire bone of interest (the proximal tibia, the distal femur, and the fibula) was included in the segmented region, manual correction using a stylus and an interactive touch-screen tablet (Cintiq 21uX, Wacom, Krefeld, Germany) was also performed.

3.3.3.2 Alignment

The CT imaging was performed in supine position; therefore, the knees were re-oriented in a neutral standing alignment (MATLAB) to match Open-MR scans of the knee (Figure 3-3- A, B). Two vectors were defined for re-alignment; one vector passed through the centroid of tibial cross-

sections in different levels. The other one passed through the centroid of femoral cross-sections up to the 2 cm distance from the joint level. This vector was closely aligned with the centroid of femoral head. The images were rotated such that the average of the two vectors was vertical. In the re-aligned images, the femoral axis and the tibial axis make the same angle with the vertical line.

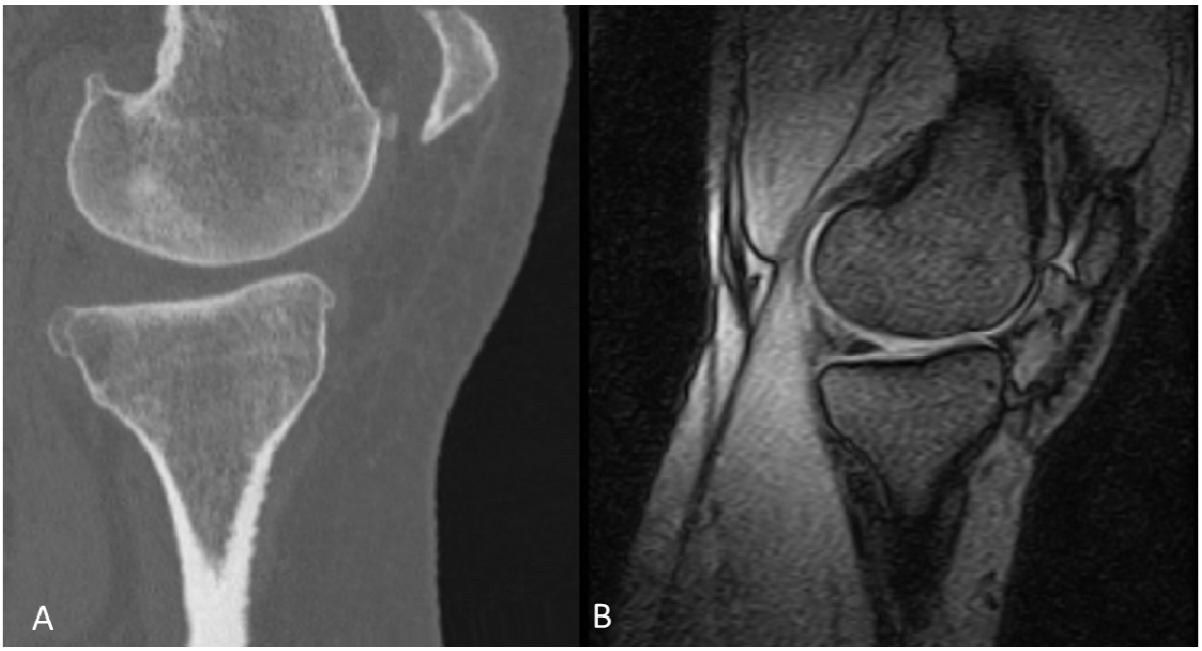

Figure 3-3- (A) Re-aligned CT image and (B) Standing MR image. CT images re-aligned such that the new alignment is similar to the standing MR images.

3.4 FE Modeling

3.4.1 Geometry

The segmented and re-aligned image were converted to a 3D polygonal surface mesh using a marching cube algorithm (ANALYZE). The 3D segmented object was imported into a reverse engineering software (GEOMAGICS) to ensure the geometry was topologically valid and did not contain holes or rough edges. However, in each image, the maximum smoothing distance was kept

less than one voxel size (0.625 mm) to maintain geometric complexity. The resultant smoothed 3D volume of the knee with surface meshing was imported into FE software (ABAQUS) (Figure 3-4). To simulate soft tissues in the knee (e.g., cartilage, meniscus), bones were surrounded by an incompressible cylindrical medium, as per McErlain et al. [36].

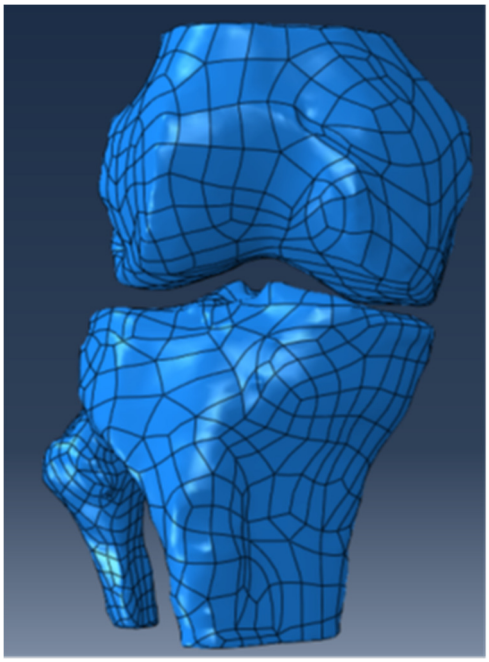

Figure 3-4- Generated 3D geometries of the femur, tibia, and fibula from CT images.

Due to the complex geometry of knee joint and to obtain a better estimate of mechanical metrics, the model was meshed using10-noded, quadratic, tetrahedral elements (Figure 3-5). The global element size for bony tissues was 2 mm. Since the focus of this study was on the bone, a larger element size was used to mesh soft tissue cylinder to reduce computational time. The size of the elements on the surface of the soft tissue cylinder was 20 mm. A convergence study was performed, and FE outcomes did not change by more than 1% when using smaller elements.

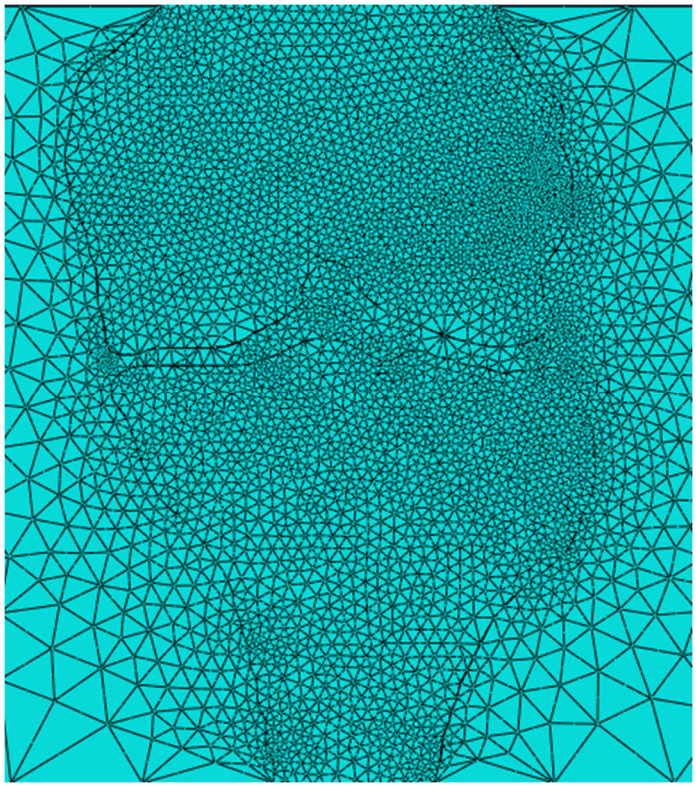

Figure 3-5- Meshed FE model with 10-noded tetrahedral elements. Image shows the femur, tibia, and soft tissue cylinder in the coronal plane.

3.4.2 Material Properties

A tibial-specific E-BMD relationship was used to convert image-based BMD to elastic modulus. Among the E-BMD relationships in the literature, Goulet's tibial trabecular-specific equation ($E = 6310(BV/TV)^{2.1}$) has been shown to be more suitable for QCT-based FE modeling of the proximal tibia [72, 79]; thus, this equation was used to map material properties to the proximal tibia as well as fibula. [79, 88]. A custom algorithm in MATLAB was used to map the obtained elastic modulus from BMD to the tetrahedral elements. Briefly, a grid of sampling points, with equal space between them, was created inside each of the elements. The elastic modulus of the image voxel containing each point was assigned to the same sampling point. The elastic modulus

of each tetrahedral element was assumed to be the average of the elastic moduli of the sampling points within the element [79] (Figure 3-6). Elastic moduli ranged from 1 MPa to around 25 GPa for elements of the proximal tibia. A high elastic modulus was assigned to the distal femur (500 GPa) to model femur as a rigid body. This decision was made after reviewing displacement patterns in the joint and to ensure that there was no extra rotation in the joint due to the lack of ligaments and tendons. Also, images of the distal femur were not full-length; therefore, the FE model failed to simulate correct load transfer to the proximal tibia with a flexible distal femur. Modeling the distal femur as a rigid body helped to overcome both of these limitations. This is a common method used with subject-specific FE modeling [11, 89, 90].

All of the elements of bony tissues had isotropic linear material properties with a Poisson's ratio of 0.3. For surrounding soft tissues, homogeneous, incompressible and isotropic material properties were applied (E=10 MPa, Poisson's ratio=0.495) [36]. This was done because only CT images were available, and subject-specific modeling of cartilage, ligaments, tendons, and meniscus was not feasible.

3.4.3 Loading and Boundary Conditions

Femur's most proximal section was fixed in all directions, except a uniform vertical displacement (1 mm). The most distal sections of the tibia and fibula were constrained for all degrees of freedom. The vertical reaction force at the top surface of femur was obtained in each FE model, and ratio of the derived reaction force to the weight of each person was used to adjust FE results according to each person's body weight.

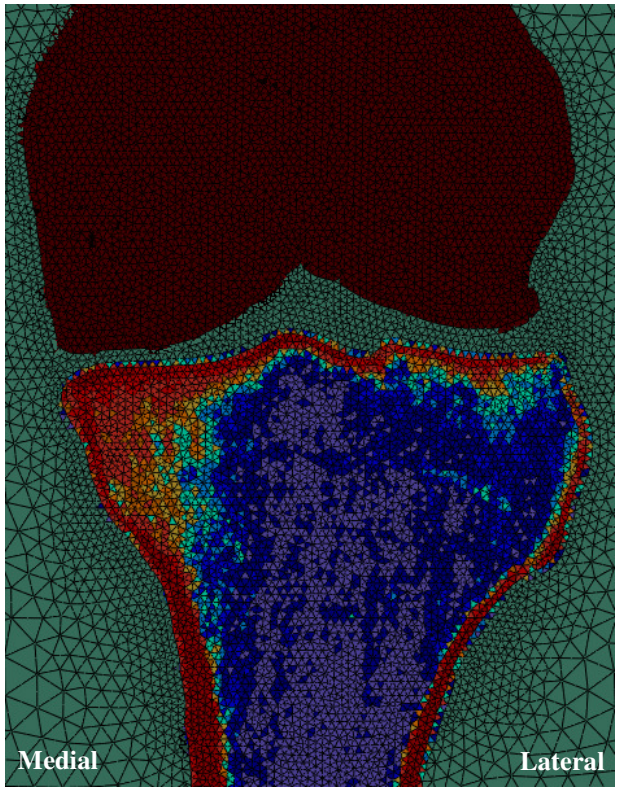

Figure 3-6- Assigned material properties for the FE model. Image-based BMD was mapped to the modulus of elasticity of the bones while an isotropic and homogeneous material was used to model soft tissue. In the image, red shows higher elastic modulus.

3.5 FE Outcomes

FE-based stiffness as well as von-Mises and minimum principal stress and strain distributions were acquired for the proximal tibia. Von-Mises strain was calculated using the following equation:

$$\varepsilon = \frac{\sqrt{2}}{3}\sqrt{(\varepsilon_1-\varepsilon_2)^2+(\varepsilon_2-\varepsilon_3)^2+(\varepsilon_3-\varepsilon_1)^2} \qquad \textit{Equation 3-1}$$

In this equation, ε_1, ε_1, and ε_1 are principal strain values.

To normalize the results based on the weight of each person, the reaction forces at the most proximal section of the femur in the FE models were obtained (ABAQUS). As a linear FE model

was used, the stress and strain values were then adjusted by the product of participant weight divided by the obtained reaction force.

Illustration of von-Mises stress, minimum principal stress, and minimum principal strain distributions as well as displacement along the axis for OA and normal knees are shown in Figure 3-7 to Figure 3-10.

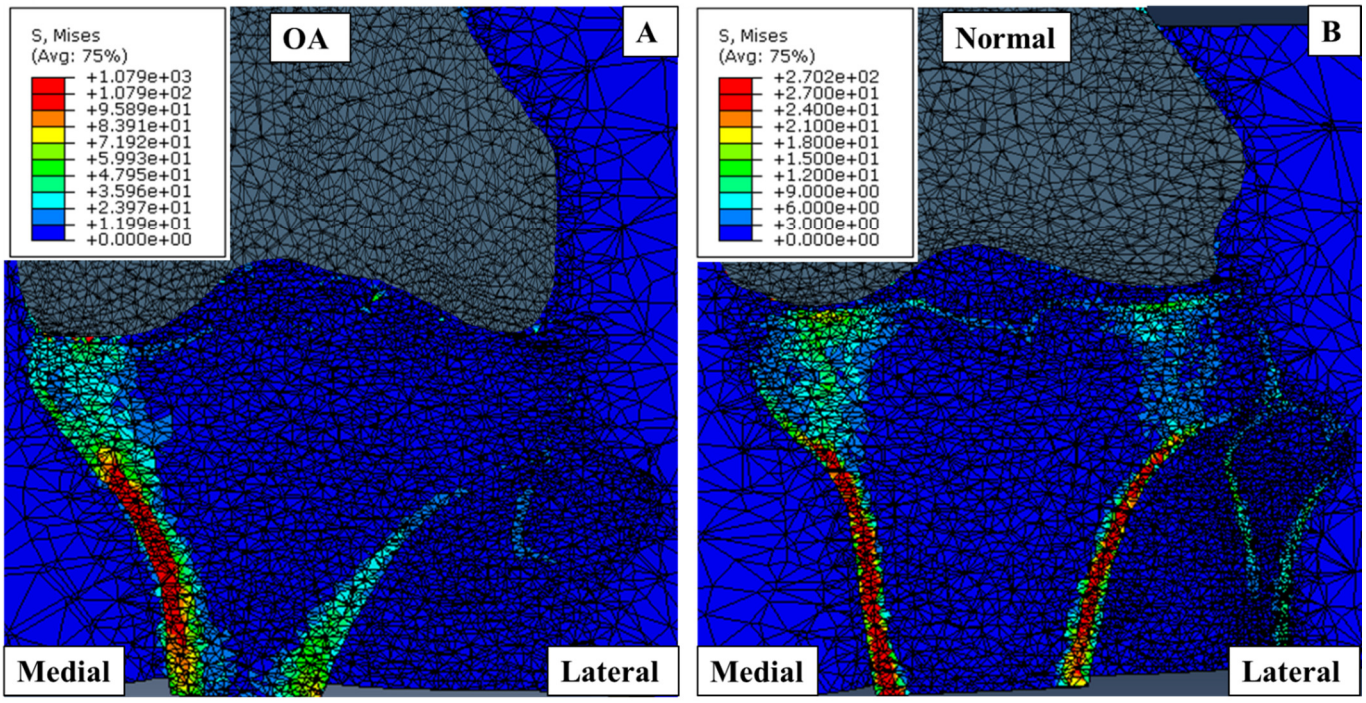

Figure 3-7- Von-Mises stress contours in an OA (A) and normal (B) proximal tibia.

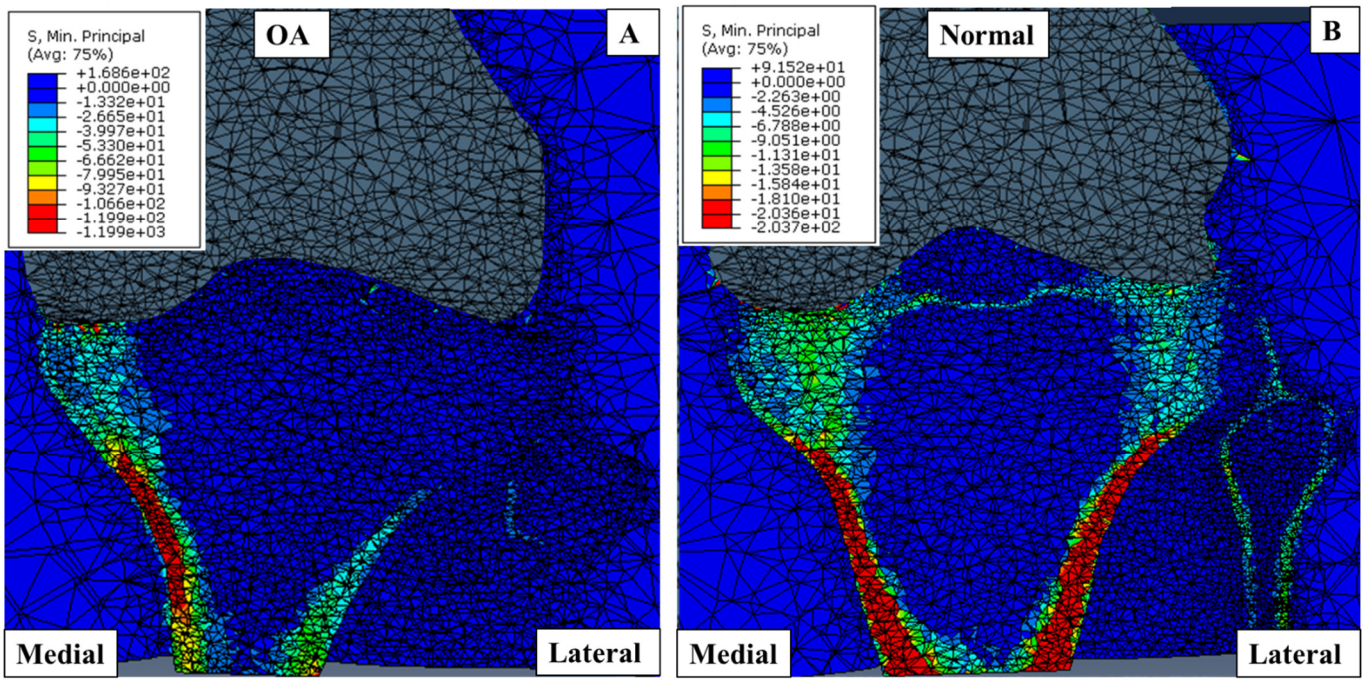

Figure 3-8- Minimum principal stress contours in an OA (A) and normal (B) proximal tibia.

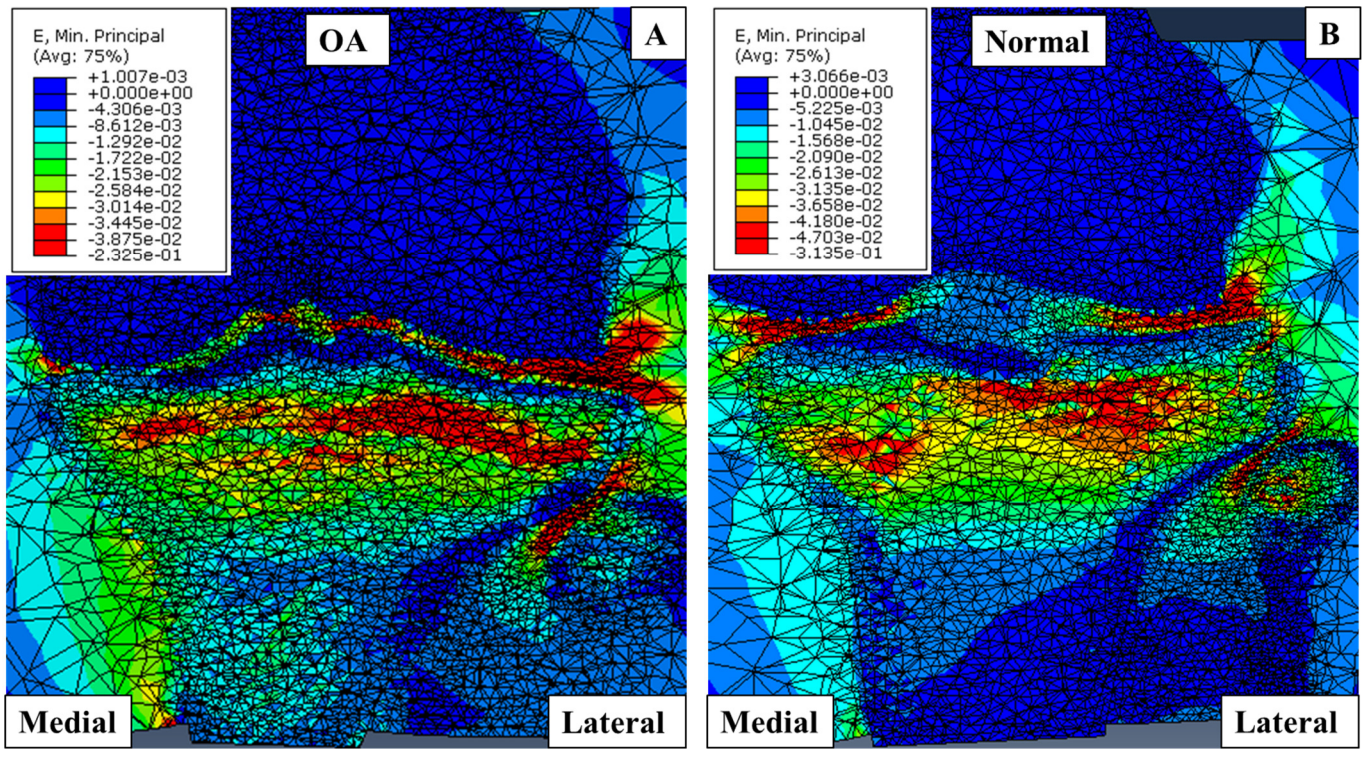

Figure 3-9- Minimum principal strain contours in an OA (A) and normal (B) proximal tibia.

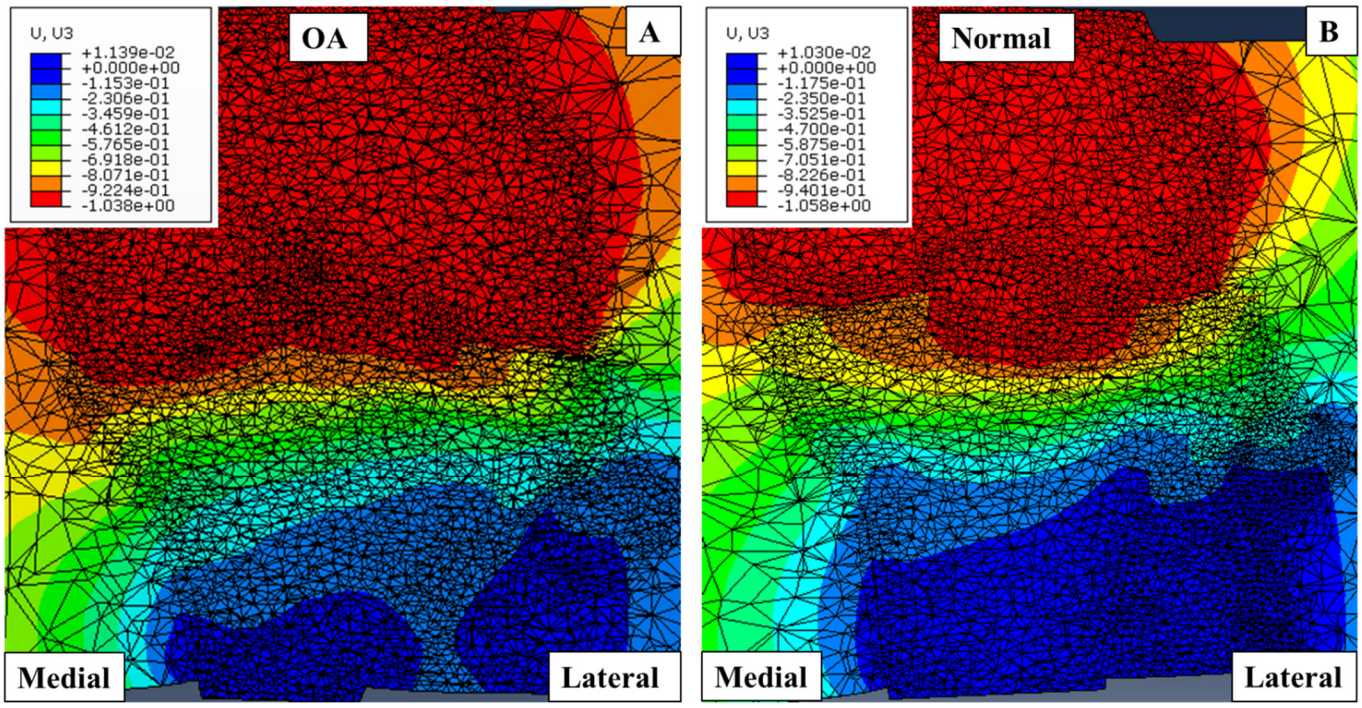

Figure 3-10- Displacement along the axis is illustrated in an OA (A) and normal (B) proximal tibia.

To ensure that modeling soft tissue and cartilage as a cylindrical medium in this study did not result in an incorrect loading distribution in the joint, an FE model with cartilage material only between the opposing bones was also developed. Results of these two different modeling approaches for soft tissue and cartilage were highly similar and shown in Figure 3-11 to Figure 3-14.

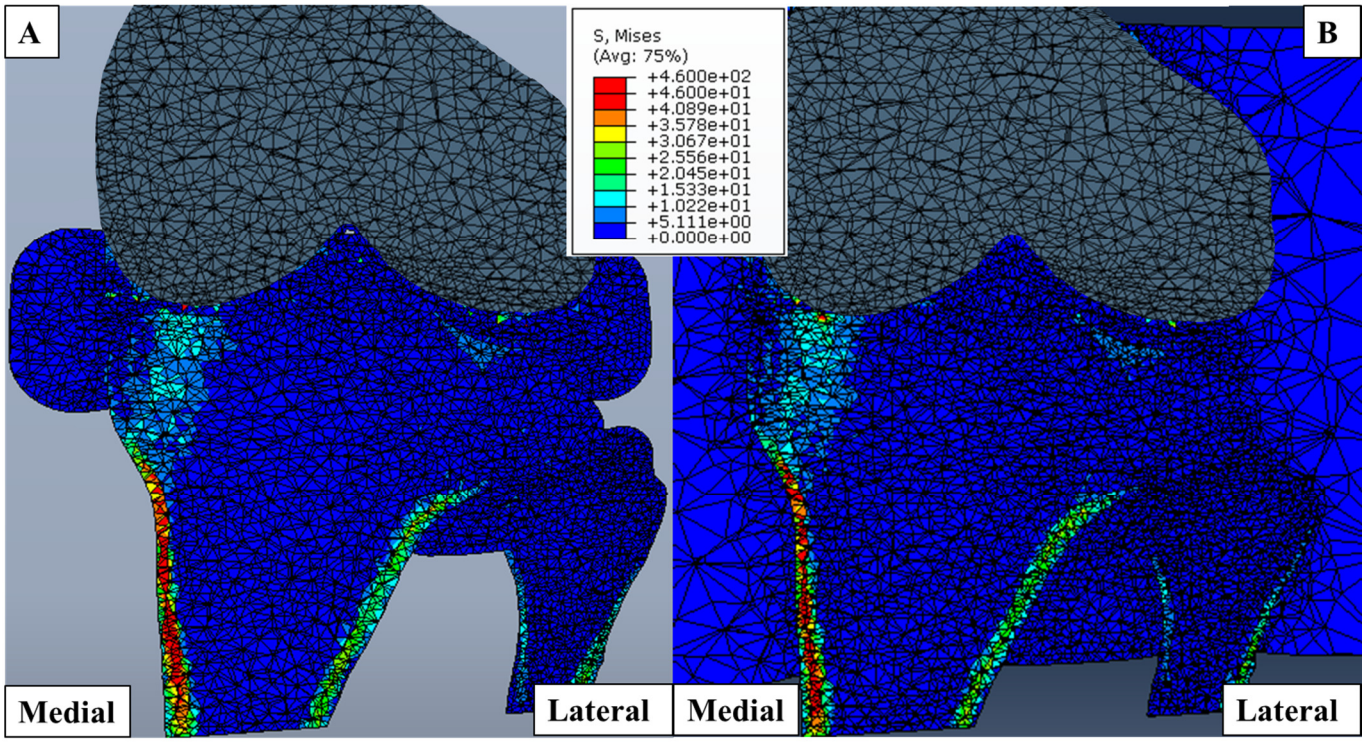

Figure 3-11- Comparison of FE-derived von-Mises stress with two different modeling approaches for soft tissue: (A) Cartilage material was only placed between the opposing bones; (B) Soft tissue and cartilage were modeled as a cylindrical medium.

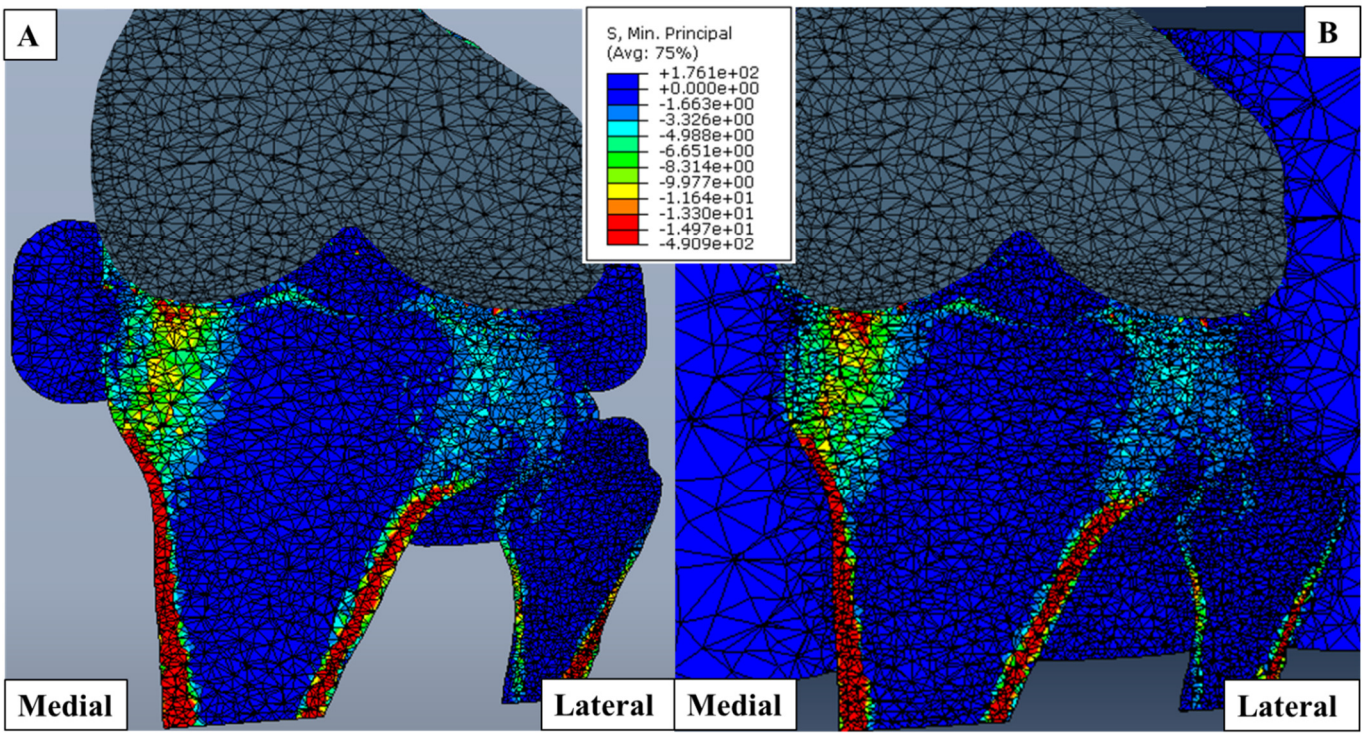

Figure 3-12- Comparison of FE-derived minimum principal stress with two different modeling approaches for soft tissue: (A) Cartilage material was only placed between the opposing bones; (B) Soft tissue and cartilage were modeled as a cylindrical medium.

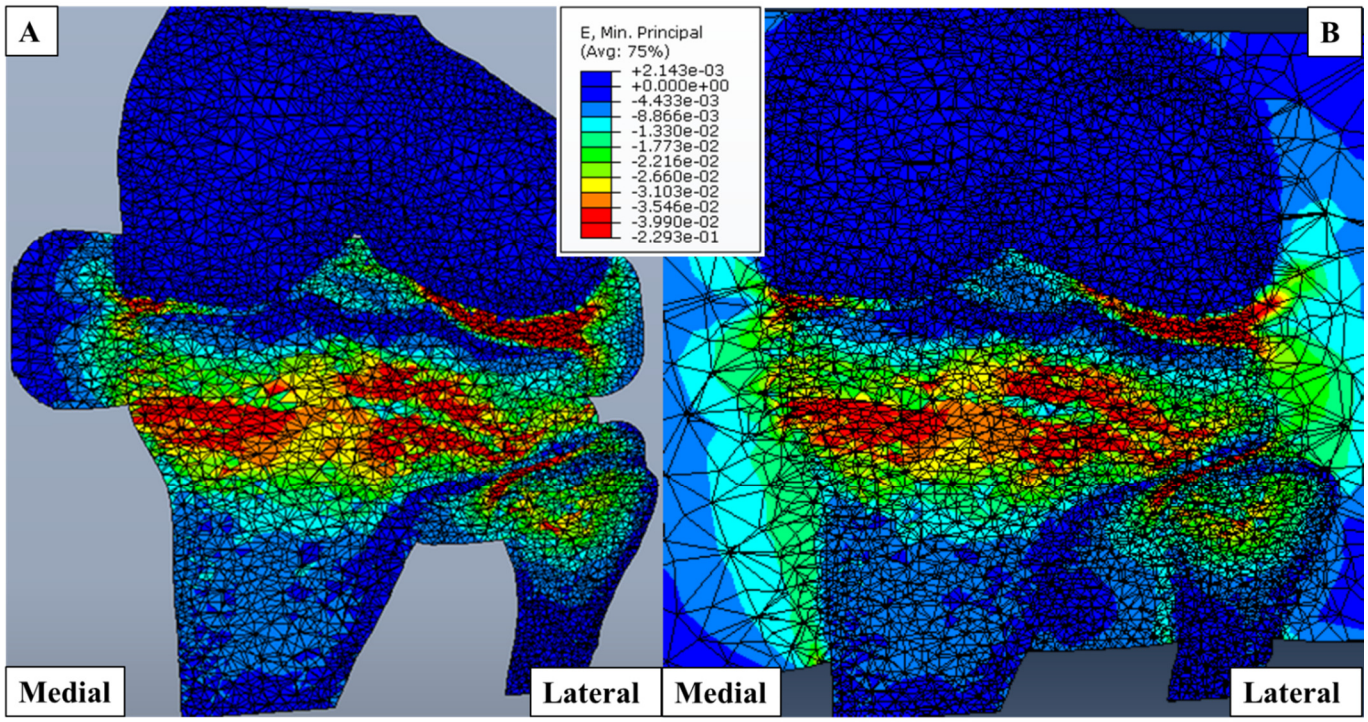

Figure 3-13- Comparison of FE-derived minimum principal strain with two different modeling approaches for soft tissue: (A) Cartilage material was only placed between the opposing bones; (B) Soft tissue and cartilage were modeled as a cylindrical medium.

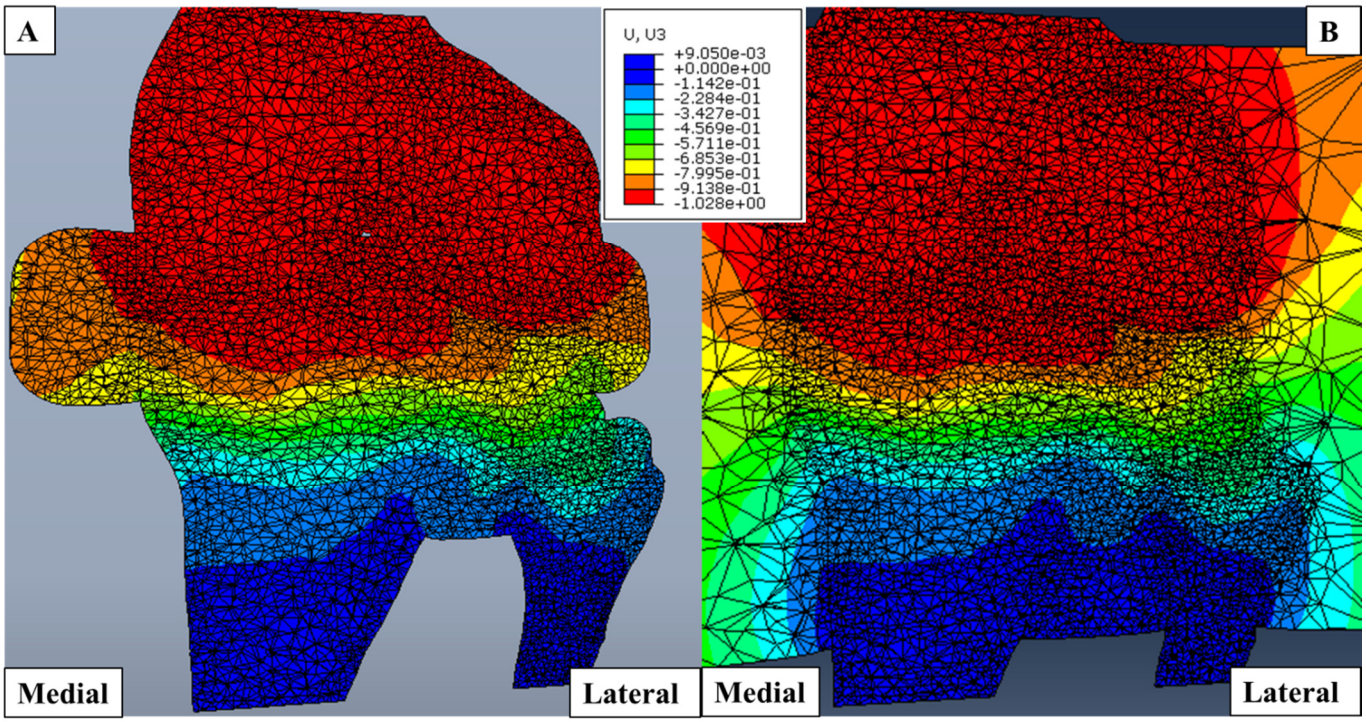

Figure 3-14- Comparison of FE-derived vertical displacement with two different modeling approaches for soft tissue: (A) Cartilage material was only placed between the opposing bones; (B) Soft tissue and cartilage were modeled as a cylindrical medium.

3.6 Regional Analysis

Different regions were defined for regional analysis of FE outcomes. The proximal tibia was divided into three different regions with 40%, 20% and 40% ratios, along the medial-lateral direction, to form the medial, central and lateral regions. Both the subchondral cortical and subchondral trabecular regions had a thickness of 2.5 mm. Subchondral cortical region started from the surface of the TF joint, and subchondral trabecular bone started at the end of subchondral cortical bone. The epiphyseal line was defined 15 mm below the lowest surface of medial or lateral compartments. The region between the end of subchondral trabecular bone and epiphyseal line was defined as epiphyseal region. Metaphyseal region started from the epiphyseal line and had a thickness of 20 mm. Figure 3-15 shows the different regions which were used to compare the FE outcomes in OA and normal proximal tibia.

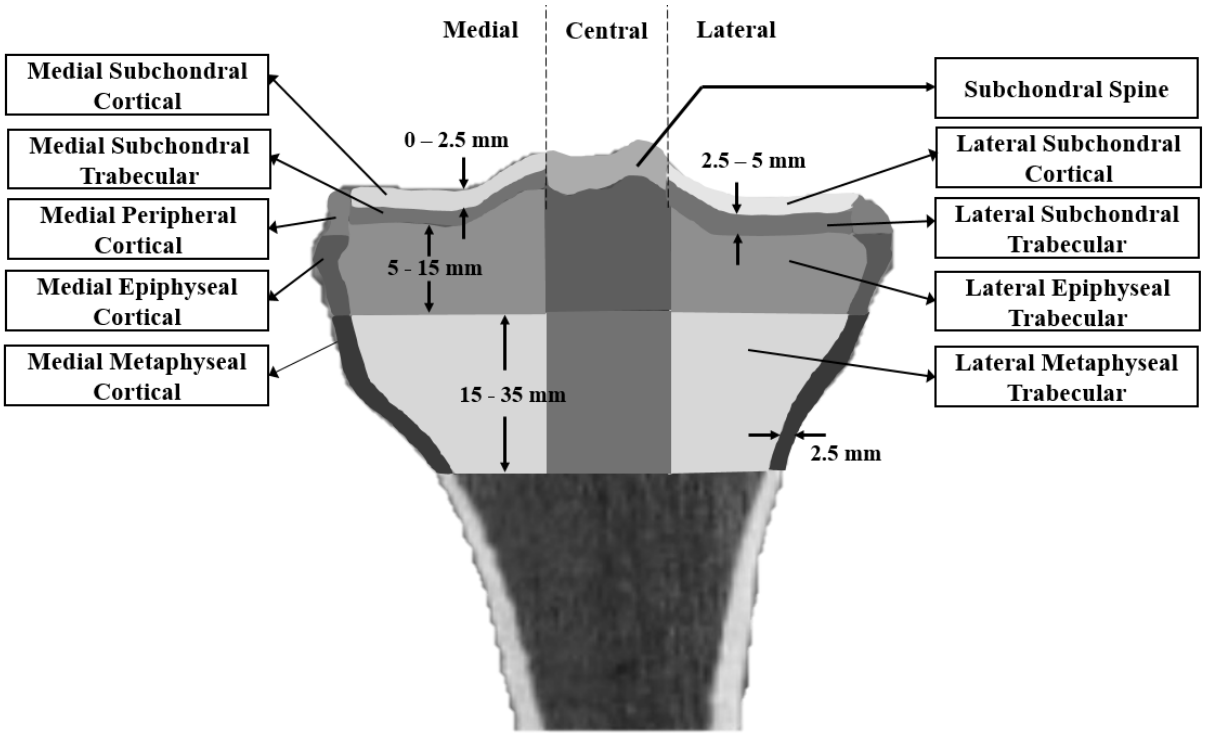

Figure 3-15- Different regions used for analyzing FE results of the proximal tibia. Lateral regions are located on the right side of the image while medial regions are at the left side of the image.

For calculating medial and lateral proximal tibial stiffness, lateral and medial compartments of the distal femur were removed, respectively, by assigning soft tissue material properties to them in ABAQUS (Figure 3-16). Stiffness of the medial and lateral compartments of the proximal tibia was calculated as the applied vertical load (derived at the top of the femur) divided by the average vertical displacement of the nodes in the respective compartments.

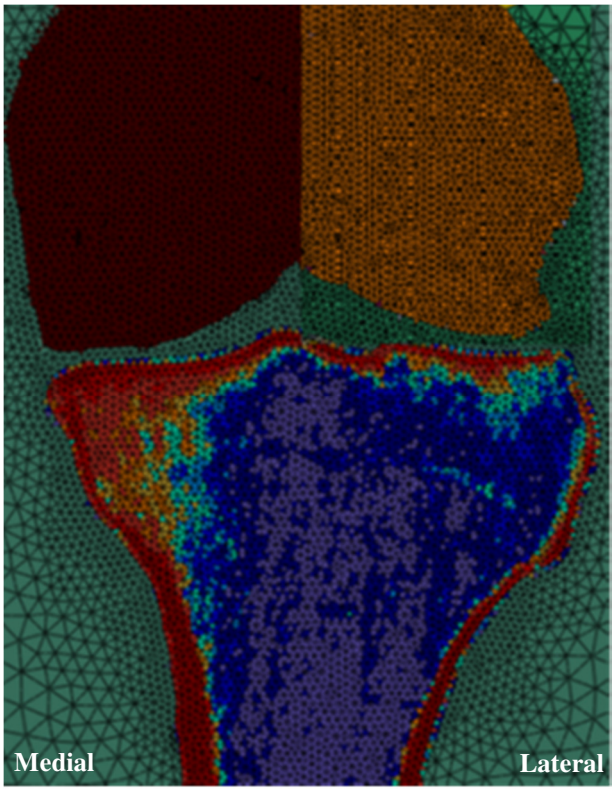

Figure 3-16- To calculate the stiffness of medial compartment of the proximal tibia, the lateral compartment was isolated by assigning soft tissue material properties to the lateral distal femur.

3.7 Statistical Analysis

3.7.1 Precision of FE models

Precision was assessed using root mean square coefficients of variation (CV%) pertaining to the 14 individuals scanned three times each using the following equation [91]:

$$CV\% = \sqrt{\frac{\sum_{j=1}^{m} \left(\frac{SD_j}{\bar{x}_j} \times 100\% \right)^2}{m}} \qquad \textit{Equation 3-2}$$

Where m was the number of participants (m=14), x_j was the mean of the three scans, and SD_j was the standard deviation of three scans for each individual obtained from following equation:

$$SD_j = \sqrt{\frac{\sum_{i=1}^{n} \left(x_{ij} - \bar{x}_j \right)^2}{n-1}} \qquad \textit{Equation 3-3}$$

In above equation, n is the number of repeated scans for each participant (n=3 in this study).

We had $m \times (n-1) = 14 \times (3-1) = 28$ degrees of freedom (DOF) for calculating precision. These DOF meet Gluer's recommendation of 27 DOF required to establish reliable precision errors with an upper 90% confidence limit less than 30% (e.g., if the precision error is 2%, we are 90% confident that the true precision error is less than 2.6%) [91].

3.7.2 Comparison Results between OA and Normal Knees

Preliminary comparisons of von-Mises stress, minimum principal stress, von-Mises strain, minimum principal strain, and stiffness values in different regions of the proximal tibia were evaluated between OA and normal knees using statistical tests, percentage differences relative to normal, percentage differences expressed in relation to CV% precision errors (e.g., percentage differences are 10 times larger than associated precision errors) and Cohen's *d* effect sizes. For each FE metric, Cohen's *d* was calculated as the difference between the two means (OA minus

normal) divided by the pooled standard deviation (SD). Pooled SD was obtained using following equation:

$$SD_{pooled} = \sqrt{\sum_{j=1}^{m} \frac{\left(SD_j\right)^2}{m}} \qquad \textit{Equation 3-4}$$

An absolute Cohen's $|d|$ larger than 0.8 was considered to be a large effect size with clinical significance [92].

To determine whether OA and normal FE outcomes were significantly different, unpaired t-tests were used with normally distributed datasets while non-parametric Mann-Whitney U-tests were used for datasets that were not normally distributed. The distribution of each FE outcome for OA and normal groups was determined by calculating the z-scores for skewness (a measure of asymmetry of the distribution) and kurtosis (a measure of the sharpness of the distribution) of the data. A variable with skewness or kurtosis z-score outside of ±1.96 limits was considered to have a non-parametric distribution. We considered an alpha level less than 0.05 to be statistically significant.

4 Results

4.1 Precision Results

4.1.1 Von-Mises Stress

Average von-Mises stress in participants with and without OA, and in different regions of the proximal tibia, ranged from 0.129 MPa to 2.231 MPa. Precision errors for von-Mises stress for both OA and normal participants ranged from 4.1% to 10.3% (average: 5.8%). CV% ranged from 3.1% to 8.0% in OA participants (average: 4.5%), and 3.7% to 9.4% (average: 5.5%) in normal participants (Table 4-1).

4.1.2 Principal Compressive Stress

Average minimum principal stress in participants with and without OA, and in different regions of the proximal tibia, ranged from -0.118 MPa to -2.058 MPa. Precision error of FE outcome of minimum principal stress for both OA and normal participants ranged from 3.7% to 10.5% (average: 6.1%) (Table 4-2). CV% ranged from 2.9% to 8.1% in OA participants (average: 4.9%) and 3.2% to 9.5% (average: 5.7%) in normal participants.

Table 4-1- Mean (±SD) of each repeated scans, mean (± SD) of all of the scans, and precision error for FE outcome of von-Mises stress in different regions of the proximal tibia.

von-Mises stress (MPa)	First scan	Second scan	Third scan	All scans	CV%
	Mean ± SD	Mean ± SD	Mean ± SD	Mean ± SD	
Medial peripheral cortical	0.425 ± 0.205	0.422 ± 0.199	0.406 ± 0.175	0.418 ± 0.192	4.9
Medial epiphyseal cortical	0.707 ± 0.368	0.711 ± 0.392	0.704 ± 0.383	0.707 ± 0.379	6.1
Medial metaphyseal cortical	2.245 ± 0.822	2.187 ± 0.824	2.262 ± 0.929	2.231 ± 0.851	6.7
Medial subchondral cortical	0.755 ± 0.179	0.757 ± 0.189	0.770 ± 0.202	0.761 ± 0.188	4.7
Medial subchondral trabecular	0.631 ± 0.170	0.632 ± 0.162	0.645 ± 0.182	0.636 ± 0.170	4.2
Medial epiphyseal trabecular	0.452 ± 0.148	0.453 ± 0.150	0.461 ± 0.167	0.455 ± 0.154	4.8
Medial metaphyseal trabecular	0.540 ± 0.258	0.564 ± 0.278	0.542 ± 0.252	0.549 ± 0.261	8.9
Subchondral spine	0.344 ± 0.109	0.349 ± 0.119	0.344 ± 0.110	0.346 ± 0.112	4.7
Epiphyseal central	0.153 ± 0.059	0.156 ± 0.060	0.152 ± 0.056	0.154 ± 0.058	7.9
Metaphyseal central	0.132 ± 0.045	0.136 ± 0.045	0.130 ± 0.042	0.129 ± 0.045	6.7
Lateral subchondral cortical	0.479 ± 0.140	0.467 ± 0.145	0.466 ± 0.136	0.471 ± 0.139	4.5
Lateral subchondral trabecular	0.347 ± 0.112	0.338 ± 0.113	0.339 ± 0.107	0.341 ± 0.110	4.8
Lateral epiphyseal trabecular	0.217 ± 0.061	0.208 ± 0.054	0.212 ± 0.055	0.212 ± 0.055	5.2
Lateral metaphyseal trabecular	0.171 ± 0.057	0.156 ± 0.043	0.162 ± 0.043	0.163 ± 0.045	10.3
Lateral peripheral cortical	0.297 ± 0.061	0.291 ± 0.059	0.294 ± 0.064	0.294 ± 0.060	4.4
Lateral epiphyseal cortical	0.337 ± 0.092	0.342 ± 0.087	0.333 ± 0.092	0.338 ± 0.089	5.7
Lateral metaphyseal cortical	0.869 ± 0.247	0.865 ± 0.237	0.847 ± 0.240	0.860 ± 0.240	4.1

Table 4-2- Mean (±SD) of each repeated scans, mean (±SD) of all scans, and precision error for FE outcome of minimum principal stress in different regions of the proximal tibia

Minimum principal stress (MPa)	First scan	Second scan	Third scan	All scans	CV%
	Mean ± SD	Mean ± SD	Mean ± SD	Mean ± SD	
Medial peripheral cortical	-0.372 ± 0.205	-0.366 ± 0.193	-0.349 ± 0.172	-0.362 ± 0.189	5.7
Medial epiphyseal cortical	-0.589 ± 0.300	-0.595 ± 0.319	-0.586 ± 0.312	-0.590 ± 0.309	6.6
Medial metaphyseal cortical	-2.071 ± 0.848	-2.012 ± 0.846	-2.092 ± 0.973	-2.058 ± 0.882	7.7
Medial subchondral cortical	-0.520 ± 0.155	-0.514 ± 0.160	-0.529 ± 0.175	-0.521 ± 0.163	3.9
Medial subchondral trabecular	-0.454 ± 0.149	-0.451 ± 0.147	-0.460 ± 0.164	-0.455 ± 0.153	3.7
Medial epiphyseal trabecular	-0.425 ± 0.146	-0.425 ± 0.148	-0.433 ± 0.164	-0.428 ± 0.152	4.8
Medial metaphyseal trabecular	-0.504 ± 0.254	-0.528 ± 0.274	-0.506 ± 0.250	-0.513 ± 0.257	8.9
Subchondral spine	-0.297 ± 0.102	-0.303 ± 0.109	-0.301 ± 0.104	-0.301 ± 0.104	5.3
Epiphyseal central	-0.142 ± 0.057	-0.145 ± 0.057	-0.142 ± 0.054	-0.143 ± 0.055	8.2
Metaphyseal central	-0.117 ± 0.042	-0.121 ± 0.043	-0.115 ± 0.039	-0.118 ± 0.041	7.3
Lateral subchondral cortical	-0.324 ± 0.090	-0.314 ± 0.087	-0.316 ± 0.090	-0.318 ± 0.088	5.0
Lateral subchondral trabecular	-0.253 ± 0.071	-0.246 ± 0.066	-0.248 ± 0.066	-0.249 ± 0.067	4.6
Lateral epiphyseal trabecular	-0.197 ± 0.055	-0.189 ± 0.049	-0.192 ± 0.049	-0.192 ± 0.050	5.3
Lateral metaphyseal trabecular	-0.156 ± 0.055	-0.142 ± 0.039	-0.148 ± 0.040	-0.149 ± 0.042	10.5
Lateral peripheral cortical	-0.215 ± 0.050	-0.214 ± 0.045	-0.216 ± 0.052	-0.215 ± 0.048	5.2
Lateral epiphyseal cortical	-0.249 ± 0.056	-0.254 ± 0.054	-0.251 ± 0.061	-0.251 ± 0.056	5.9
Lateral metaphyseal cortical	-0.711 ± 0.223	-0.709 ± 0.210	-0.688 ± 0.204	-0.703 ± 0.210	5.2

4.1.3 Von-Mises Strain

Average von-Mises strain in participants with and without OA, and in different regions of the proximal tibia, ranged from 550 to 2400 microstrain. Root mean square CV% of von-Mises strain for both OA and normal participants ranged from 3.1% to 7.6% (average: 5.1%) (Table 4-3). CV% ranged from 1.9% to 5.7% in OA participants (average: 3.7%), and 2.6% to 8.8% (average: 5.0%) in normal participants.

4.1.4 Principal Compressive Strain

Average minimum principal strain in participants with and without OA, and in different regions of the proximal tibia, ranged from 563 to 2688 microstrain. Root mean square CV% of minimum principal strain for both OA and normal participants ranged from 3.2% to 7.6% (average: 5.5%) (Table 4-4). CV% ranged from 1.9% to 6.0% in OA participants (average: 4.0%), and 2.7% to 8.8% (average: 5.3%) in normal participants.

Table 4-3- Mean (±SD) of each repeated scans, mean (± SD) of all scans, and precision error for FE outcome of von-Mises strain in different regions of the proximal tibia.

von-Mises strain (microstrain)	First scan	Second scan	Third scan	All scans	CV%
	Mean ± SD	Mean ± SD	Mean ± SD	Mean ± SD	
Medial peripheral cortical	1151 ± 534	1134 ± 511	1085 ± 428	1123 ± 488	5.6
Medial epiphyseal cortical	1342 ± 584	1342 ± 594	1305 ± 517	1330 ± 563	3.9
Medial metaphyseal cortical	1053 ± 383	1070 ± 413	1062 ± 412	1062 ± 400	4.6
Medial subchondral cortical	559 ± 212	542 ± 195	548 ± 205	550 ± 203	4.9
Medial subchondral trabecular	778 ± 326	742 ± 303	753 ± 301	758 ± 308	5.8
Medial epiphyseal trabecular	2167 ± 823	2110 ± 797	2117 ± 761	2131 ± 792	3.6
Medial metaphyseal trabecular	1929 ± 795	1948 ± 844	1940 ± 828	1939 ± 820	4.4
Subchondral spine	797 ± 364	788 ± 416	778 ± 334	788 ± 368	6.7
Epiphyseal central	2417 ± 786	2395 ± 816	2386 ± 764	2400 ± 787	3.1
Metaphyseal central	1719 ± 705	1731 ± 710	1733 ± 710	1728 ± 706	4.4
Lateral subchondral cortical	818 ± 332	861 ± 341	830 ± 320	837 ± 328	6.0
Lateral subchondral trabecular	1224 ± 422	1259 ± 431	1242 ± 418	1242 ± 421	4.8
Lateral epiphyseal trabecular	2261 ± 770	2298 ± 832	2261 ± 751	2273 ± 781	3.7
Lateral metaphyseal trabecular	1804 ± 791	1704 ± 722	1765 ± 718	1758 ± 734	7.2
Lateral peripheral cortical	1100 ± 458	1144 ± 506	1147 ± 487	1130 ± 481	5.1
Lateral epiphyseal cortical	1082 ± 392	1089 ± 402	1108 ± 394	1093 ± 391	5.6
Lateral metaphyseal cortical	695 ± 324	642 ± 265	674 ± 262	670 ± 281	7.6

Table 4-4- Mean (±SD) of each repeated scans, mean (± SD) of all scans, and precision error for FE outcome of minimum principal strain in different regions of the proximal tibia.

Minimum principal strain (microstrain)	First scan	Second scan	Third scan	All scans	CV%
	Mean ± SD	Mean ± SD	Mean ± SD	Mean ± SD	
Medial peripheral cortical	1219 ± 570	1197 ± 533	1140 ± 444	1185 ± 512	6.1
Medial epiphyseal cortical	1424 ± 626	1423 ± 633	1383 ± 551	1410 ± 601	4.2
Medial metaphyseal cortical	1123 ± 400	1138 ± 431	1130 ± 431	1130 ± 418	4.7
Medial subchondral cortical	576 ± 217	552 ± 193	560 ± 204	563 ± 203	5.6
Medial subchondral trabecular	795 ± 342	752 ± 314	765 ± 317	770 ± 322	6.5
Medial epiphyseal trabecular	2447 ± 936	2379 ± 905	2390 ± 866	2405 ± 900	3.7
Medial metaphyseal trabecular	2153 ± 905	2177 ± 962	2166 ± 939	2166 ± 933	4.7
Subchondral spine	837 ± 397	831 ± 458	821 ± 365	830 ± 403	7.2
Epiphyseal central	2706 ± 878	2681 ± 912	2676 ± 855	2688 ± 879	3.2
Metaphyseal central	1888 ± 790	1901 ± 794	1902 ± 794	1897 ± 789	4.9
Lateral subchondral cortical	842 ± 332	888 ± 346	855 ± 323	862 ± 330	6.4
Lateral subchondral trabecular	1301 ± 449	1340 ± 459	1324 ± 445	1321 ± 447	5.2
Lateral epiphyseal trabecular	2493 ± 852	2538 ± 918	2494 ± 822	2508 ± 860	3.9
Lateral metaphyseal trabecular	1992 ± 893	1880 ± 812	1948 ± 814	1940 ± 829	7.5
Lateral peripheral cortical	1121 ± 468	1173 ± 519	1176 ± 499	1157 ± 492	5.7
Lateral epiphyseal cortical	1093 ± 407	1100 ± 413	1123 ± 405	1105 ± 403	5.9
Lateral metaphyseal cortical	695 ± 334	643 ± 271	674 ± 269	670 ± 288	7.4

4.1.5 Structural Stiffness

Mean structural stiffness for both OA and normal participants was 7708 N/mm in the medial and 5959 N/mm in the lateral compartment. Root mean square CV% of structural stiffness for both OA and normal participants was 3.6% in the medial compartment and 5.0% in the lateral compartment (Table 4-5). CV% in OA participants was 3.3% and 2.9% for the medial and lateral compartments, respectively. In the normal participants, CV% was 3.1% for the medial, and 5.5% for the lateral compartment.

Table 4-5- Mean (±SD) of each repeated scans, mean (±SD) of all scans, and precision error for structural stiffness in medial and lateral compartments.

Stiffness (N/mm)	First scan	Second scan	Third scan	All scans	CV%
	Mean ± SD	Mean ± SD	Mean ± SD	Mean ± SD	
Medial compartment	7784 ± 3037	7644 ± 2971	7697 ± 6636	7708 ± 2986	3.6
Lateral compartment	5931 ± 1531	6044 ± 1748	5902 ± 1419	5959 ± 1545	5.0

4.2 Preliminary Comparisons of OA and Normal FE Outcomes

4.2.1 Von-Mises Stress

Von-Mises stress for different regions of proximal tibia ranged from 0.136 MPa to 2.791 MPa in OA bone and 0.121 MPa to 1.671 MPa in normal bone (Table 4-6). Mapped representations of von-Mises stress results onto CT images of the proximal tibia are shown in Figure 4-1. Overall stress was higher in OA versus normal bone. The percent difference in von-Mises stress was as high as +101% in the medial peripheral cortical bone (~21x CV%), and +113% in the medial epiphyseal cortical region (~18x CV%). Average values of von-Mises stress in OA and normal bone are displayed in Figure 4-2. Also, the percent differences of von-Mises stress in OA and normal bone are shown in Figure 4-3. Regions with significant difference are shown with red outline (p-value < 0.05).

Table 4-6- Von-Mises stress mean (±SD), the difference (absolute and percent) relative to normal, p-value, and effect size (Cohen's d) of von-Mises stress in various regions of the proximal tibia between normal and osteoarthritic bone. Regions with significant differences are highlighted in the table (p-value < 0.05).

von-Mises stress (MPa)	OA-group	Normal-group	Difference		p-value	Cohen's *d*
	Mean ± SD	Mean ± SD	Absolute	Percent		
Medial peripheral cortical	0.558 ± 0.165	0.277 ± 0.083	0.281	101.3%	0.002	1.46
Medial epiphyseal cortical	0.962 ± 0.345	0.453 ± 0.204	0.510	112.6%	0.006	1.34
Medial metaphyseal cortical *	2.791 ± 0.872	1.671 ± 0.281	1.120	67.0%	0.025	1.31
Medial subchondral cortical	0.860 ± 0.193	0.662 ± 0.126	0.198	30.0%	0.042	1.06
Medial subchondral trabecular	0.736 ± 0.175	0.536 ± 0.094	0.200	37.2%	0.021	1.17
Medial epiphyseal trabecular *	0.539 ± 0.177	0.372 ± 0.062	0.167	44.8%	0.048	1.08
Medial metaphyseal trabecular *	0.684 ± 0.303	0.413 ± 0.113	0.271	65.6%	0.064	1.04
Subchondral spine	0.426 ± 0.074	0.265 ± 0.081	0.160	60.4%	0.002	1.44
Epiphyseal central	0.171 ± 0.032	0.137 ± 0.074	0.034	25.1%	0.281	0.60
Metaphyseal central	0.136 ± 0.027	0.121 ± 0.059	0.016	13.0%	0.530	0.35
Lateral subchondral cortical	0.526 ± 0.166	0.415 ± 0.085	0.112	26.9%	0.139	0.80
Lateral subchondral trabecular	0.369 ± 0.140	0.314 ± 0.069	0.055	17.6%	0.368	0.50
Lateral epiphyseal trabecular	0.221 ± 0.063	0.204 ± 0.050	0.016	8.0%	0.601	0.30
Lateral metaphyseal trabecular	0.169 ± 0.040	0.157 ± 0.053	0.012	7.4%	0.651	0.26
Lateral peripheral cortical	0.333 ± 0.054	0.255 ± 0.039	0.078	30.5%	0.009	1.29
Lateral epiphyseal cortical	0.391 ± 0.091	0.284 ± 0.047	0.107	37.5%	0.018	1.20
Lateral metaphyseal cortical	0.943 ± 0.290	0.778 ± 0.156	0.165	21.3%	0.209	0.69

(*) shows regions which were not normally distributed whereby Mann-Whitney U-tests were used to compare stress between normal and OA bone.

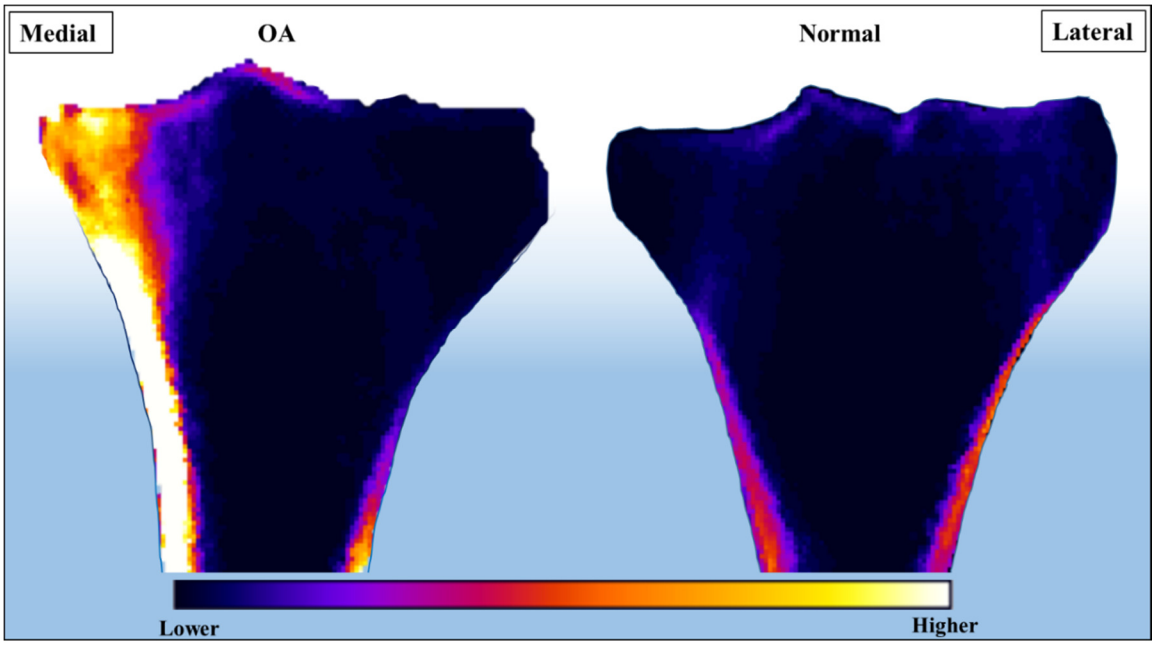

Figure 4-1- Von-Mises stress of OA and normal proximal tibia are demonstrated in coronal section of CT image. Yellow indicates high stress while black is low stress.

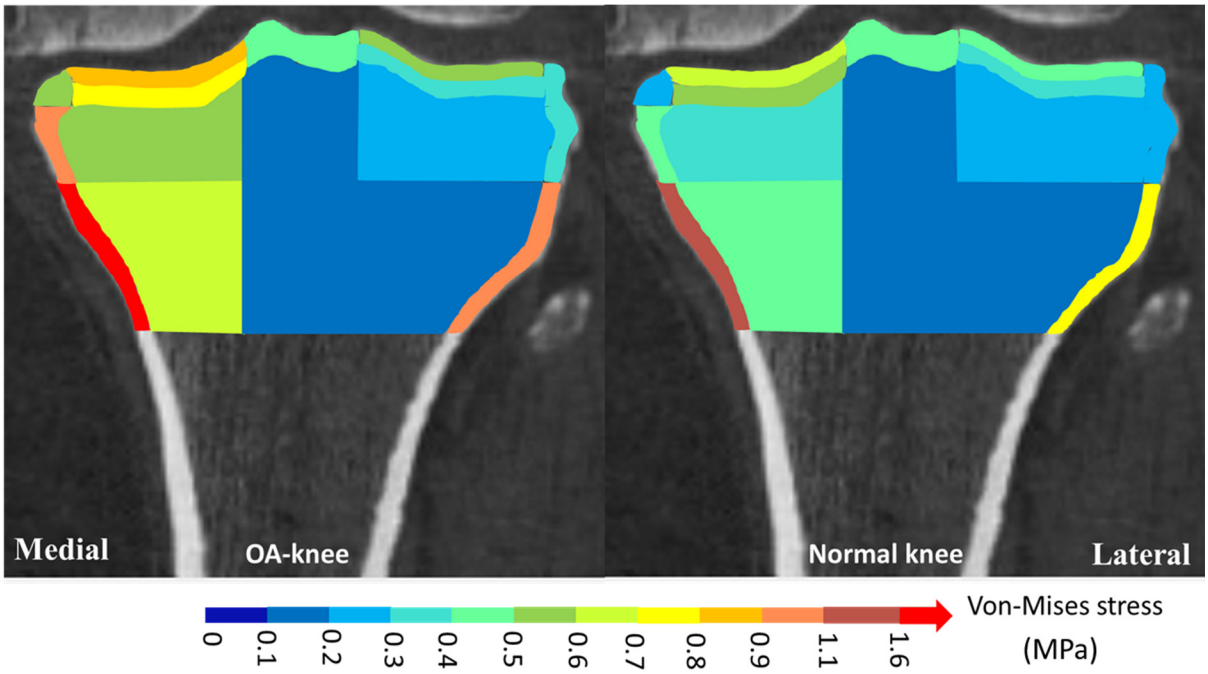

Figure 4-2- Average von-Mises stress values (MPa) are shown in different regions of OA and normal proximal tibia.

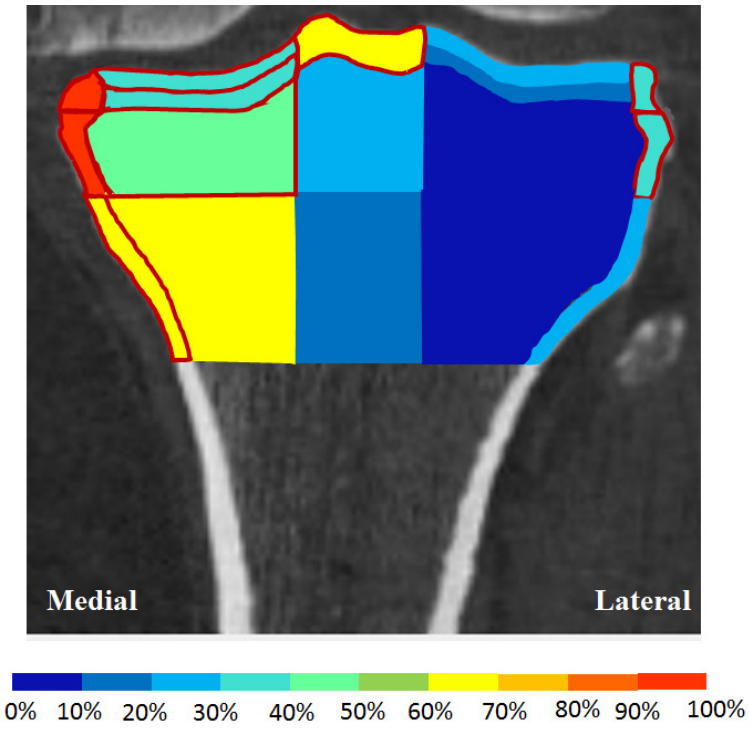

Figure 4-3- Percent differences of von-Mises stress in normal and OA proximal tibia. The differences are significant in regions with red outline ($p<0.05$).

4.2.2 Principal Compressive Stress

Minimum principal stress for different regions of proximal tibia ranged from -2.607 MPa to -0.126 MPa in OA bone and -0.121 MPa to -1.452 MPa in normal bone (Table 4-7). The difference in minimum principal stress was as high as -106% in the medial peripheral cortical bone (~19x CV%) and -107% in the medial epiphyseal cortical region (~16x CV%). Average values of minimum principal stress in OA and normal bone are displayed in Figure 4-4. Also, the percent differences of principal compressive stress in OA and normal bone are shown in Figure 4-5. Regions with significant difference are shown with red outline (p-value < 0.05).

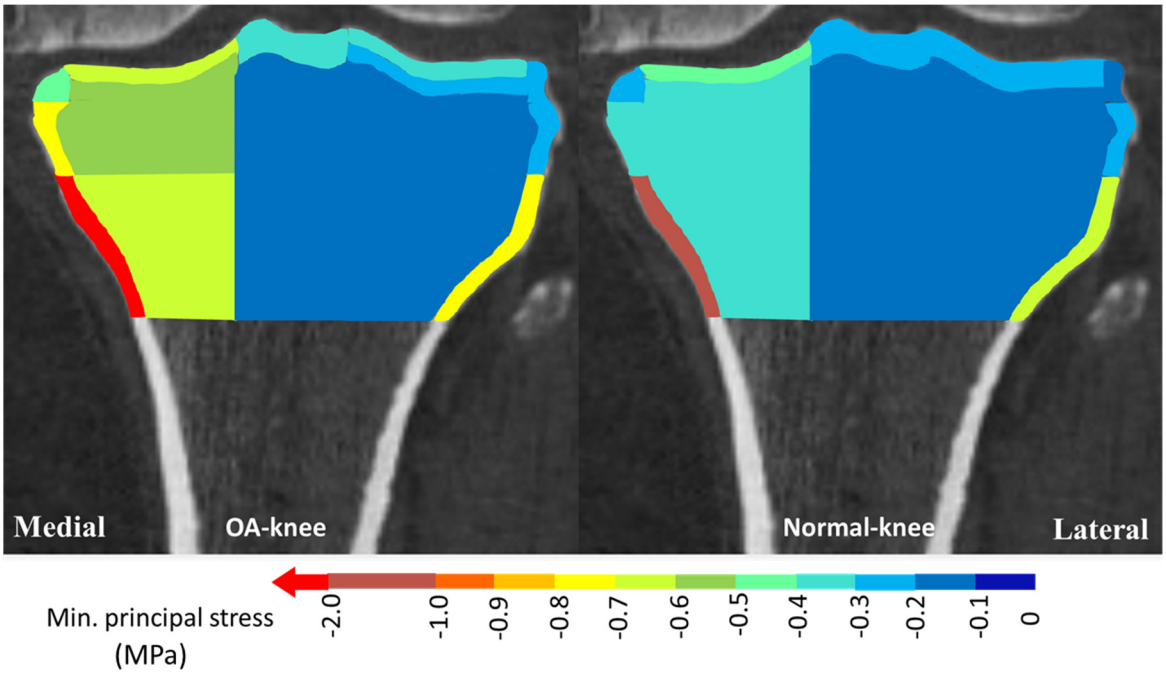

Figure 4-4- Average minimum principal stress values (MPa) are shown in different regions of OA and normal proximal tibia.

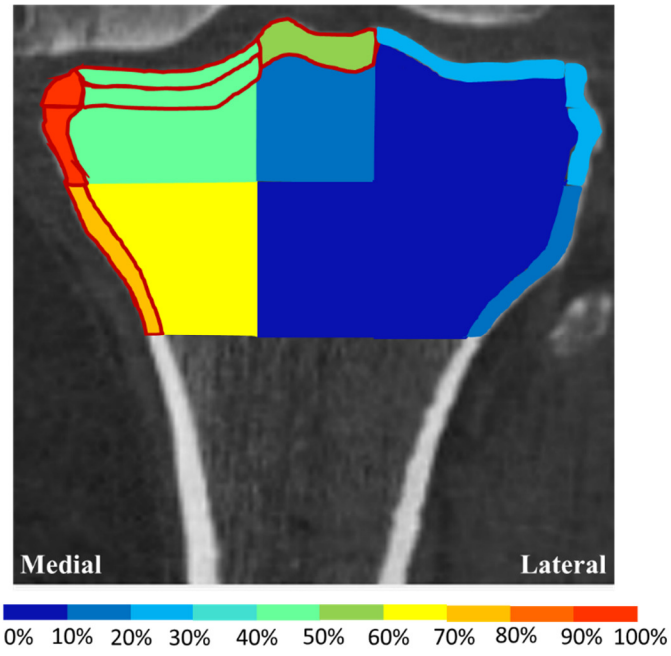

Figure 4-5- Percent differences of minimum principal stress in normal and OA proximal tibia. The differences are significant in regions with red outline ($p<0.05$).

Table 4-7- Minimum principal stress mean (±SD), difference (absolute and percent) relative to normal, p-value, and effect size (Cohen's d) of minimum principal stress in different regions of the proximal tibia between normal and osteoarthritic bone. Regions with significant differences are highlighted in the table (p<0.05).

Minimum principal stress (MPa)	OA-group	Normal-group	Difference		p-value	Cohen's *d*
	Mean ± SD	Mean ± SD	Absolute	Percent		
Medial peripheral cortical *	-0.494 ± 0.178	-0.240 ± 0.080	-0.254	-106.0%	0.006	1.36
Medial epiphyseal cortical	-0.796 ± 0.283	-0.384 ± 0.165	-0.412	-107.2%	0.006	1.33
Medial metaphyseal cortical *	-2.607 ± 0.949	-1.452 ± 0.271	-1.155	-79.5%	0.013	1.28
Medial subchondral cortical *	-0.622 ± 0.175	-0.423 ± 0.058	-0.199	-46.9%	0.018	1.22
Medial subchondral trabecular *	-0.543 ± 0.170	-0.371 ± 0.063	-0.172	-46.4%	0.035	1.13
Medial epiphyseal trabecular *	-0.506 ± 0.178	-0.350 ± 0.061	-0.156	-44.7%	0.085	1.03
Medial metaphyseal trabecular *	-0.644 ± 0.302	-0.387 ± 0.101	-0.257	-66.5%	0.064	1.01
Subchondral spine	-0.374 ± 0.074	-0.238 ± 0.076	-0.135	-56.9%	0.005	1.35
Epiphyseal central	-0.157 ± 0.031	-0.140 ± 0.069	-0.017	-12.3%	0.559	0.33
Metaphyseal central	-0.126 ± 0.025	-0.121 ± 0.053	-0.005	-3.8%	0.838	0.12
Lateral subchondral cortical	-0.352 ± 0.106	-0.287 ± 0.058	-0.066	-22.8%	0.175	0.74
Lateral subchondral trabecular	-0.261 ± 0.081	-0.246 ± 0.063	-0.015	-6.3%	0.698	0.22
Lateral epiphyseal trabecular	-0.199 ± 0.057	-0.194 ± 0.053	-0.006	-3.0%	0.847	0.11
Lateral metaphyseal trabecular	-0.154 ± 0.039	-0.157 ± 0.055	0.003	-2.2%	0.896	0.07
Lateral peripheral cortical	-0.242 ± 0.052	-0.198 ± 0.042	-0.044	-22.4%	0.104	0.87
Lateral epiphyseal cortical	-0.285 ± 0.058	-0.228 ± 0.043	-0.057	-25.2%	0.057	1.00
Lateral metaphyseal cortical	-0.756 ± 0.248	-0.645 ± 0.165	-0.111	-17.1%	0.346	0.53

(*) shows regions which were not normally distributed whereby Mann-Whitney U-tests were used to compare stress between normal and OA bone.

4.2.3 Von-Mises Strain

Von-Mises strain for different regions of proximal tibia ranged from 573 microstrains to 2587 microstrains in OA bone and 526 microstrains to 2212 microstrains in Normal bone (Table 4-8). No difference was observed in von-Mises strain values between OA and normal knee ($p>0.05$). The highest von-Mises strain was observed in the epiphyseal central region for both normal and OA proximal tibia.

4.2.4 Principal Compressive Strain

Minimum principal strain for different regions of proximal tibia ranged from 591 microstrains to 2873 microstrains in OA bone and 534 microstrains to 2503 microstrains in normal bone (Table 4-9). No difference was observed in minimum principal strain values between OA and normal knee ($p>0.05$). The highest principal compressive strain was in the epiphyseal central for both normal and OA proximal tibia.

4.2.5 Structural Stiffness

Average structural stiffness in the medial compartment was 8515 N/mm in OA bone and 6902 N/mm in normal bone. In the lateral compartment, the structural stiffness was 6200 N/mm and 5718 N/mm in OA and normal bone, respectively (Table 4-10). No differences were observed in the structural stiffness of medial and lateral condyles of proximal tibia between OA and normal participants ($p>0.05$).

Table 4-8- Von-Mises strain mean (±SD), difference (absolute and percent) relative to normal, p-value, and effect size (Cohen's d) of von-Mises strain in different regions of the proximal tibia between normal and osteoarthritic bone.

von-Mises strain (microstrain)	OA-group	Normal-group	Difference		p-value	Cohen's *d*
	Mean ± SD	Mean ± SD	Absolute	Percent		
Medial peripheral cortical	1077 ± 531	1169 ± 478	-92	-7.8%	0.740	0.19
Medial epiphyseal cortical	1368 ± 635	1291 ± 530	78	6.0%	0.808	0.14
Medial metaphyseal cortical	1167 ± 427	956 ± 373	211	22.0%	0.344	0.53
Medial subchondral cortical *	573 ± 260	526 ± 142	47	9.0%	0.949	0.23
Medial subchondral trabecular *	855 ± 388	660 ± 182	195	29.5%	0.406	0.63
Medial epiphyseal trabecular *	2332 ± 995	1931 ± 523	401	20.8%	0.482	0.51
Medial metaphyseal trabecular	2113 ± 962	1765 ± 677	349	19.8%	0.448	0.43
Subchondral spine *	875 ± 492	700 ± 184	174	24.9%	0.749	0.47
Epiphyseal central	2587 ± 917	2212 ± 646	376	17.0%	0.393	0.48
Metaphyseal central	1880 ± 819	1575 ± 595	306	19.4%	0.440	0.43
Lateral subchondral cortical	895 ± 413	778 ± 233	117	15.0%	0.526	0.36
Lateral subchondral trabecular	1405 ± 514	1079 ± 239	326	30.3%	0.153	0.78
Lateral epiphyseal trabecular *	2550 ± 913	1996 ± 555	554	27.8%	0.225	0.71
Lateral metaphyseal trabecular	1888 ± 832	1627 ± 661	261	16.0%	0.528	0.36
Lateral peripheral cortical *	1263 ± 638	997 ± 228	265	26.6%	0.565	0.55
Lateral epiphyseal cortical	1176 ± 466	1010 ± 314	165	16.3%	0.452	0.42
Lateral metaphyseal cortical	663 ± 273	677 ± 310	-14	-2.0%	0.932	0.05

(*) shows regions which were not normally distributed whereby Mann-Whitney U-tests were used to compare strain between normal and OA bone.

Table 4-9- Minimum principal strain mean (±SD), difference (absolute and percent) relative to normal, p-value, and effect size (Cohen's d) of minimum principal strain in different regions of the proximal tibia between normal and osteoarthritic bone.

Minimum principal strain (microstrain)	OA-group	Normal-group	Difference		p-value	Cohen's *d*
	Mean ± SD	Mean ± SD	Absolute	Percent		
Medial peripheral cortical	1135 ± 561	1236 ± 497	-101	-8.2%	0.727	0.20
Medial epiphyseal cortical	1435 ± 666	1385 ± 582	50	3.6%	0.883	0.08
Medial metaphyseal cortical	1247 ± 433	1014 ± 399	233	23.0%	0.316	0.56
Medial subchondral cortical *	591 ± 258	534 ± 143	58	10.8%	0.949	0.28
Medial subchondral trabecular*	873 ± 405	667 ± 189	206	30.8%	0.338	0.64
Medial epiphyseal trabecular *	2626 ± 1133	2184 ± 599	442	20.2%	0.406	0.49
Medial metaphyseal trabecular	2361 ± 1096	1970 ± 771	391	19.8%	0.455	0.42
Subchondral spine *	926 ± 544	734 ± 186	192	26.2%	0.848	0.48
Epiphyseal central	2873 ± 1015	2503 ± 752	370	14.8%	0.454	0.42
Metaphyseal central	2053 ± 921	1741 ± 668	312	17.9%	0.482	0.39
Lateral subchondral cortical	914 ± 410	809 ± 249	106	13.1%	0.571	0.32
Lateral subchondral trabecular	1495 ± 548	1148 ± 249	347	30.2%	0.154	0.78
Lateral epiphyseal trabecular *	2812 ± 1006	2204 ± 611	608	27.6%	0.180	0.71
Lateral metaphyseal trabecular	2080 ± 948	1800 ± 738	280	15.6%	0.549	0.34
Lateral peripheral cortical *	1281 ± 657	1032 ± 236	248	24.1%	0.848	0.50
Lateral epiphyseal cortical	1181 ± 475	1030 ± 337	151	14.7%	0.506	0.37
Lateral metaphyseal cortical	656 ± 274	685 ± 323	-30	-4.3%	0.857	0.10

(*) shows regions which were not normally distributed whereby Mann-Whitney U-tests were used to compare strain between normal and OA bone.

Table 4-10- Structural stiffness mean (±SD), difference (absolute and percent) relative to normal, p-value, and effect size (Cohen's d) of stiffness in medial and lateral compartments of the proximal tibia between OA and normal bone.

Regional Stiffness (N/mm)	OA-group	Normal-group	Difference		p-value	Cohen's *d*
	Mean ± SD	Mean ± SD	Absolute	Percent		
Medial compartment	8515 ± 3767	6902 ± 1902	1613	23.4%	0.332	0.54
Lateral compartment	6200 ± 1201	5718 ± 1896	482	8.4%	0.580	0.31

4.2.6 Critical Limits

From the FE analysis, we also acquired maximum stress and strain limits which 2% of the elements exceeded this limit (e.g., 2% of elements in OA bone exceeded a von-Mises stress of 4 MPa). Results of this analysis are shown in Table 4-11. For OA bone, the 2% limits for von-Mises stress and minimum principal stress were significantly higher compared to normal bone. Conversely, the 2% strain limits were similar between the two groups ($p>0.05$) (Table 4-11).

Table 4-11- Mean (±SD), the difference (absolute and percent) relative to normal, p-value, and effect size (Cohen's d) of stress and strain limits of 2% volume of the proximal tibia in normal and osteoarthritic bone.

2% limits	OA-group		Normal-group		Difference		p-value	Cohen's *d*
	Mean	± SD	Mean	± SD	Absolute	Percent		
Von-Mises stress	4.026	±0.932	2.670	±0.257	1.355	50.8%	0.003	1.41
Minimum principal stress	4.095	±0.981	2.706	±0.266	1.389	51.4%	0.004	1.39
Von-Mises strain	4537	±1590	3752	±1147	785	20.9%	0.310	0.56
Minimum principal strain	5227	±1806	4367	±1352	859	19.7%	0.333	0.54

5 Discussion

5.1 Overview of Findings

This study evaluated the *in vivo* precision of FE-derived outcomes of mechanical stiffness and stress/strain distributions in knees of healthy participants and those with OA. This is the first study to report the *in vivo* precision of mechanical outcomes of the proximal tibia. This is also the first subject-specific FE modeling study to identify mechanical metrics which potentially differentiate OA and normal bone.

This developed FE tool provides precise measures of von-Mises stress, minimum principal stress, von-Mises strain, and minimum principal strain in the different regions of the proximal tibia (Average CV% < 6.1%). The calculated precision errors in all of the regions were less than 11%. Calculated FE-based structural stiffness of the medial or lateral compartment were also precise and had precision errors less than 5%. Our precision errors are in the same range as previously reported CV% precision errors for FE modeling using high-resolution peripheral QCT imaging (HR-pQCT) to obtain bone stiffness and stress [93, 94]. Low precision errors are due to many factors. First, the methodology for obtaining BMD, which was converted to the elastic modulus of bone using E-BMD relationships, was accurate [95-100]. Second, the images were realigned to ensure that the loading axis was the same for all three different positions. Third, the same regions were used to compare the FE results between different positions. Fourth, the modeling approaches were verified based upon convergence/sensitivity studies.

On average, von-Mises stress of the proximal tibia were 65% (~11x CV%) larger on the medial side of OA bone compared to normal bone. Similarly, the minimum principal stress was 70% (~12x CV%) larger in medial side of the OA bone. Overall, the difference in stress was as high as 21 times the precision error for von-Mises stress, and 19 times the precision error for

minimum principal stress. These differences are large, particularly when compared to metrics such as least significant change (LSC). LSC is mostly used to determine if skeletal changes have occurred over time, and for a two-sided 95% confidence of interval (95% CI), LSC is equal to 2.77 times the precision. Although we were studying two different groups here (OA and normal), and not the change over time, comparing the differences with LSC could be useful in identifying the actual differences (which are not just because of measurement errors) between the two groups. If the observed difference in an outcome between OA and normal bone is higher than LSC (2.77x CV%), this outcome could be potentially used to differentiate OA and normal bone.

The regions with statistically significant differences were similar for both von-Mises stress and minimum principal stress. It is worthwhile to note that although the medial epiphyseal trabecular regions did not have significantly different minimum principal stress, the p-values of the minimum principal stress in this region was close to the p-values of von-Mises stress.

No difference was observed between von-Mises strain, minimum principal strain, and structural stiffness. Inspecting Cohen's *d* for stiffness revealed that there was a high variability in stiffness among each group, which makes it unreliable to detect differences between OA and normal bone.

The 2% strain limit was similar for both OA and normal groups (5227 and 4367 microstrain, respectively). These strain limits, as well as strain values in different regions of the tibia, were below the failure strain for cortical (9500 microstrain) and trabecular bone (7000 microstrain) [101, 102]. With regards to stress, 2% of the volume was stressed beyond 4.1 MPa for OA bone and beyond 2.7 MPa for normal bone. The difference in the 2% stress limit was significant and approximately 16 times the CV%. Unlike failure strain limit, the ultimate strength of bone is highly dependent on bone density [102, 103]. More specifically, the ultimate strength

of bone is related to BMD cubed. Previous research has reported an average yield stress as of 5.8±3.4 MPa for trabecular bone in the normal proximal tibia [102]. Although FE-based stress of the cancellous bone in the different regions of the proximal tibia were lower than the failure stress, failure limit could be different for the OA proximal tibia due to different bone density. Comparing stress values and failure stress limits of different regions of OA proximal tibia and also deriving safety factors for individual elements could give more insight into the failure risk of OA bone in various regions.

Although speculative, it is worth hypothesizing on why stress is higher in OA knees. We believe this is due to combined effects of various factors, including: (1) higher weight; (2) malalignment; and (3) altered BMD in OA knees. First, OA participants in this study had significantly higher weight compared to the normal participants, which could contribute to the observed higher stress in OA knees. It is worthwhile to note that although the difference in weight of OA and normal groups was significant (p-value<0.05), it was much lower than the observed differences in stress values. Second, regarding to the alignment, OA knees were slightly varus which could also contribute to different stress values in normal and OA models. Third, although the differences in BMD values were not significant [104], the BMD differences could also affect the stress distribution in normal and OA knees. Using Goulet's equation for material mapping [72], elastic modulus in FE models is related to $BMD^{2.1}$, and is more sensitive to BMD alterations. Altered elastic modulus can affect the stress values and distributions in OA and normal knees. Finally, while stress was different between two groups, no difference was observed in the strain values. Similar strain levels could be an indication of bone adaptation in response to altered loading in OA joint and higher stress values in OA bone.

5.2 Comparison to Existing Findings

Results of this study have not been validated, and validating strain values with *in situ* experimental tests is an aim of future research. However, comparing results with existing literature and *in-vivo* data shows that FE outcomes are quite reliable. FE-derived outcomes are in agreement with other published FE analyses [36, 59, 105]. The reported von-Mises stress values are within the same range as previous subject-specific FE modeling of the knee joint by McErlain et al. [36] and an FE study of the proximal tibia by Tuncer et al. [105] with similar loading conditions. Also, the obtained strain values in this research compare favorably with the strain range reported for FE modeling of the proximal tibia [105]. The calculated stiffness for the proximal tibia are similar to the structural stiffness reported in a previous study by our research group [59].

5.3 Study Strengths

First, a main Strength of this study was using CT images of study participants as opposed to idealized geometries that resemble the knee joint. The heterogeneity of bone is also considered using E-BMD relationships, which has been shown to affect the predictive ability of QCT-based FE models [79, 106]. This *in vivo* FE modeling technique enables us to compare mechanical FE outcomes in people with and without OA and associate these outcomes to pain levels and other features of OA (e.g., cysts, osteophytes). Also, this methodology can be used to study links between different OA factors (e.g., physical activity, alignment), which are not known in cadaveric samples, and various FE-derived mechanical properties.

Second, this study met the conservative number of the patients and repeated scans per patient as proposed by Gluer et al., to obtain precision errors with small confidence intervals (CI) (90% confidence with a confidence interval of 30%) [91]. Additionally, we had an equal number of participants with and without knee OA (7 OA, 7 normal). The precision error was calculated for

both OA and normal group independently, and for the total participants; thus, developed FE models can be used precisely to compare mechanical metrics between OA and normal knees.

5.4 Study Limitations

Limitations of this study pertain to small sample size, using isotropic material properties for bone, using a single E-BMD equation for cortical and trabecular bone, and simplified modeling of soft tissue as well as cartilage.

First, in order to have an independent precision error for normal and OA knees, with the same confidence interval as the combined group, we need twice as many participants (14 normal, and 14 OA). Since the precision errors of the separate groups were very similar, we merged the two groups and found the precision error for the combined group. With this decision, Gluer's recommendation was met without unnecessary radiation exposure of more participants.

Second, although bone is orthotropic (transversely isotropic), isotropic material properties were assumed for trabecular and cortical bone in the FE models. Taking into account the varied properties in different directions might also improve the predictive ability of the FE models. However, previous studies show that ignoring orthotropic material property assignment in modeling large bone has little effect on the results [106]. Therefore, for the purpose of comparing the FE metrics between OA and normal, and to simplify our modeling for possible clinical applications, inhomogeneous isotropic material property assignment is a reasonable modeling simplification.

Third, a single E-BMD relationship was used to assign material properties to the cortical and trabecular bone. While this approach is common in the literature, applying cortical-specific and trabecular-specific E-BMD relationships improves the predictive ability of the QCT-FE

models [79]. Using cortical-specific and trabecular-specific E-BMD relationships require separate segmentation of each bone, and it would be expensive timewise. This is an aim of future research.

Fourth, all tissues in the FE models were considered to be linearly elastic materials; thus, mechanical stiffness was independent of loading conditions. However, in reality, bone and cartilage have viscoelastic properties in which the stiffness is also affected by loading rate.

Fifth, only CT images were available; therefore, subject-specific modeling of cartilage, ligaments, tendons, and meniscus was not feasible. To overcome this limitation, a cylinder of tissue with an isotropic homogeneous material was used to model cartilage and soft tissue of the knee joint. However, cartilage molecular composition of collagen fibers and proteoglycan media makes it highly inhomogeneous and anisotropic. Since the focus of the study was on bone mechanical behavior, using simplified material properties for cartilage was justified.

Sixth, to avoid any complications associated with the modeling contact surface in the joint, soft tissue cylinder and the proximal tibia, the distal femur, and the fibula were assumed to be bonded completely without any relative motion in their interface. Future research aiming to simulate study findings should strive to model contact.

Seventh, due to the lack of the ligaments and tendons in the FE models, the distal femur was modeled as a non-deformable rigid body, and it was allowed to move only along its axis to avoid non-physiological motion in the joint. While the assumption of non-deformable rigid bodies for the distal femur provides stability to the knee joint in the absence of ligaments, any intraosseous (within bone) information for the distal femur is disregarded in this approach. If this information is needed, the proximal tibia and fibula should be modeled as rigid bodies with the reversed boundary conditions (i.e. fixed boundary on the most proximal section of the distal femur, and unit displacement on the most distal sections of the proximal tibia and fibula).

Eighth, another limitation of this study was assigning the same material properties for cartilage in normal and OA knees. Previous studies show that stiffness and thickness of the articular cartilage layer largely affect stress in the bone [107]. Defects in the cartilage layer and cartilage loss present in the OA could increase the stress in the bone. However, assuming same material properties for the OA and normal cartilage produces conservative results. In other words, if subject-specific cartilage material properties were used, we would reasonably expect to see more differences in von-Mises stress between OA and normal bone.

Ninth, to compare the results of different mechanical outcomes between OA and normal knees, multiple statistical tests were performed and the significance value (p-value) was reported for each outcome. However, we had low statistical power because of the small sample size. Since this study was a preliminary work to report the precision and explore potential differences between OA and normal bone, use of a small sample was justified. Nevertheless, to draw a more definite conclusion, statistical tests should be performed on larger sample sizes.

Tenth, a p-value of 0.05 was used in this study to identify regions with significantly different FE outcomes in OA and normal bone. However, Bonferroni adjustments should be used to account for multiple statistical tests. Bonferroni adjustments are performed using a modified p-value which is equal to the original p-value divided by the number of statistical tests (e.g., with 2 tests the modified p-value should be 0.025). Since this study was a preliminary comparison of FE outcomes between OA and normal bone, with the aim of identifying potentially differentiating outcomes, Bonferroni adjustments were not performed.

Eleventh, CT images for this study were from middle of the tibia to middle of the femur, and full-length images were not available. To ensure that the loading axis for all of the participants and all three different positions of each participant were equivalent, the images were rotated by an

angle obtained using a custom algorithm in MATLAB for each image. Though, the images for different positions of each person were not perfectly aligned, and this could contribute to the precision errors. However, since our precision errors were within the same range as previous FE studies in the literature, the alignment approach presented in this research is satisfactory for the purpose of this study. To fully overcome this limitation, full-length images are required. Though, these images will lead to higher radiation exposure. Another possibility is using reduced volume CT images, which have the same radiation dose as a 2D radiograph, but they also could be used to measure limb alignment [108].

6 Conclusion and Future Directions

6.1 Conclusions

Our objectives in this study were to 1) Develop a subject-specific FE modeling methodology for the OA and normal knee joint; 2) Determine the *in vivo* precision of proximal tibia stiffness and stress/strain distributions offered using FE, and 3) Determine whether FE-derived metrics discriminate normal and OA knees.

Objective 1 was met by developing 3D subject-specific FE model using CT images and material properties obtained from CT images and published E-BMD relationships. Objective 2 was achieved by evaluating stress, strain, stiffness values in the proximal tibia of 14 individuals (7 with knee OA, 7 without) who have been imaged three times each (for assessing precision). Objective 3 was achieved via a preliminary comparison of OA (n=7) and normal (n=7) knees. The comparison consisted of statistical tests, percentage differences between groups, percentage differences expressed in relation to precision errors, as well as Cohen's *d* effect sizes [109].

The outcome of Objective 1 was subject-specific FE modeling methodology and model specific to each patient. This allowed us to model each knee based on individual geometry obtained from CT images. CT-based FE modeling is important as clinical information (i.e., pain symptoms, etc.) can only be obtained from people living with OA. The outcomes from Objective 2 included precision values for quantitative measures of stiffness and stress/strain. This information helps us identify which FE-derived outcomes are repeatable and best-suited for objective 3. The results of Objective 3 were mechanical properties of the proximal tibia which potentially differ between OA and normal knee.

Results of this study indicates that:

1. FE modeling has the potential to precisely quantify and differentiate mechanical property variations in normal and OA knees, *in vivo*.
2. OA and normal bone exhibit dissimilar stress levels but similar strain levels.
3. Structural stiffness values had large variability and failed to discriminate OA and normal bone.

6.2 Contributions

Using subject-specific FE modeling, we were able to study the combined effects of various mechanical and morphological alterations of bone on mechanical metrics in people with OA. We assessed different FE outcomes of the proximal tibia between OA and normal bone. Our results show that mechanical stress is significantly higher on the medial side of the osteoarthritic proximal tibia. This is important because we were able to differentiate OA and normal proximal tibia, *in vivo*, and in early stages of OA. No difference was observed in comparing the BMD values in the same CT images [104]. Therefore, this study shows that mechanical stress is more sensitive to OA compared to BMD. We also compared strain and stiffness outcomes, which failed to find any significant differences between OA and normal bone. This study suggests that stress patterns may be more important than previously thought, and could reveal more insights into the role of bone in OA.

6.3 Clinical Significance

FE modeling of the knee joint offers an invaluable tool to monitor stress patterns in subchondral bone, which could be a factor in OA initiation and pain. Since stress is more sensitive to OA than BMD, examining the stress pattern in bone can be used for early diagnosis of OA. Results of this research provide a validated tool which could help to clarify the role of subchondral bone in

initiation and progression of OA. For example, the developed FE modeling approach could be used to investigate associations between mechanical metrics and OA-related pain. Knowing the source of pain in OA could open new methods in OA treatment and improve the quality of life for many people. Another application of this technique is in knee replacement surgeries to evaluate the mechanical interplay between bone and implant (a factor adversely associated with surgery failure), and to monitor bone alteration after surgeries. The FE tool can also be used to investigate effects of a particular treatment for knee joint abnormalities on stress patterns in bone. It might also have potential application in drug therapy to study the effect of different drugs on the mechanical properties of bone.

6.4 Future Research

1- One area for possible future work is using MR images, co-registered to the CT images, to obtain the geometry and material properties of the soft tissue which were simplified in this study. Using a similar approach to one provided here for modeling cartilage and soft tissue, and including them in the FE model with heterogeneous and deformable bone tissue, a full knee joint could be developed. Combining this full knee joint model with multi-body dynamics of the knee joint could lead to more realistic loading and boundary conditions of at the knee [110, 111]. Since ligaments and tendons could prevent non-physiological relative rotation of the femur and the tibia, more relaxed boundary conditions can be applied on the distal femur. Deformable heterogeneous material properties can also be assigned to the femur to study its intraosseous properties whereas, in this study, a non-deformable material property was applied to the distal femur to overcome the lack of ligaments and to ensure physiological load transfer to the proximal tibial surface.

2- In this study, only trabecular-specific equations were used to assign material properties of the proximal tibia. Cortical- specific and trabecular-specific E-BMD relationships could be used to map bone density to the elastic modulus. This requires segmenting the cortical and trabecular regions of the bone in the CT images. This work is currently ongoing with a new PhD student (Mehrdad Hosseini).

3- In this study, precision was calculated for different FE outcomes; however, it is unclear whether these outcomes accurately represent the mechanical behavior of the proximal tibia. The strain values could be validated using *in situ* experimental testing of the knee joint.

4- In this study, a preliminary comparison of FE outcomes was conducted between OA and normal knees, and precise FE outcomes were identified to discriminate OA and normal knees. Analysis of these outcomes, and investigating their associations with different OA symptoms, including pain, presence of osteophytes, and subchondral cyst, are areas for future work.

References

1. *Arthritis in Canada: An Ongoing Challenge*, 2003, Health canada: Ottawa (ON). p. H39-4/14-2003E.
2. Lawrence RC, Felson DT, Helmick CG, Arnold LM, Choi H, Deyo RA, et al., *Estimates of the prevalence of arthritis and other rheumatic conditions in the United States. Part II.* Arthritis Rheum, 2008. 58(1): p. 26-35.
3. Burr DB, *The importance of subchondral bone in osteoarthrosis.* Curr Opin Rheumatol, 1998. 10(3): p. 256-62.
4. Burr DB, *The importance of subchondral bone in the progression of osteoarthritis.* J Rheumatol Suppl, 2004. 70: p. 77-80.
5. Bobinac D, Spanjol J, Zoricic S, and Maric I, *Changes in articular cartilage and subchondral bone histomorphometry in osteoarthritic knee joints in humans.* Bone, 2003. 32(3): p. 284-90.
6. Brown TD, Radin EL, Martin RB, and Burr DB, *Finite element studies of some juxtarticular stress changes due to localized subchondral stiffening.* Journal of biomechanics, 1984. 17(1): p. 11-24.
7. Bjurholm A, Kreicbergs A, Brodin E, and Schultzberg M, *Substance P- and CGRP-immunoreactive nerves in bone.* Peptides, 1988. 9(1): p. 165-71.
8. Buma P, *Innervation of the patella. An immunohistochemical study in mice.* Acta Orthop Scand, 1994. 65(1): p. 80-6.
9. Schipplein OD and Andriacchi TP, *Interaction between Active and Passive Knee Stabilizers during Levelwalking.* Journal of Orthopaedic Research, 1991. 9(1): p. 113-19.
10. Mootanah R, Imhauser CW, Reisse F, Carpanen D, Walker RW, Koff MF, et al., *Development and validation of a computational model of the knee joint for the evaluation of surgical treatments for osteoarthritis.* Comput Methods Biomech Biomed Engin, 2014. 17(13): p. 1502-17.
11. Farrokhi S, Keyak JH, and Powers CM, *Individuals with patellofemoral pain exhibit greater patellofemoral joint stress: a finite element analysis study.* Osteoarthritis and Cartilage, 2011. 19(3): p. 287-94.
12. Mcerlain DD, Ulici V, Darling M, Gati JS, Pitelka V, Beier F, et al., *An in vivo investigation of the initiation and progression of subchondral cysts in a rodent model of secondary osteoarthritis.* Arthritis Res Ther, 2012. 14(1): p. R26.
13. Tozburun S, Stahl CD, Hutchens TC, Lagoda GA, Burnett AL, and Fried NM, *Continuous-wave infrared subsurface optical stimulation of the rat prostate cavernous nerves using a 1490-nm diode laser.* Urology, 2013. 82(4): p. 969-73.
14. Williams PL and Gray H, *Gray's anatomy*. 37th ed1989, Edinburgh: Churchill Livingstone. 1598 p.
15. Li G, Yin J, Gao J, Cheng TS, Pavlos NJ, Zhang C, et al., *Subchondral bone in osteoarthritis: insight into risk factors and microstructural changes.* Arthritis research & therapy, 2013. 15(6): p. 223.
16. Radin EL and Rose RM, *Role of Subchondral Bone in the Initiation and Progression of Cartilage Damage.* Clinical Orthopaedics and Related Research, 1986(213): p. 34-40.
17. Radin EL, Swann DA, Paul IL, and Mcgrath PJ, *Factors influencing articular cartilage wear in vitro.* Arthritis and rheumatism, 1982. 25(8): p. 974-80.

18. Abernethy PJ, Townsend PR, Rose RM, and Radin EL, *Is chondromalacia patellae a separate clinical entity?* The Journal of bone and joint surgery British volume, 1978. 60-B(2): p. 205-10.
19. Fortier LA and Nixon AJ, *Distributional changes in substance P nociceptive fiber patterns in naturally osteoarthritic articulations.* The Journal of rheumatology, 1997. 24(3): p. 524-30.
20. Johnston JD, *Development of a novel non-invasive imaging technique for characterizing subchondral bone density and stiffness*, 2010, The University of British Columbia
21. Imhof H, Breitenseher M, Kainberger F, Rand T, and Trattnig S, *Importance of subchondral bone to articular cartilage in health and disease.* Top Magn Reson Imaging, 1999. 10(3): p. 180-92.
22. Madry H, Van Dijk CN, and Mueller-Gerbl M, *The basic science of the subchondral bone.* Knee Surgery Sports Traumatology Arthroscopy, 2010. 18(4): p. 419-33.
23. Lo GH, Mcalindon TE, Niu J, Zhang Y, Beals C, Dabrowski C, et al., *Bone marrow lesions and joint effusion are strongly and independently associated with weight-bearing pain in knee osteoarthritis: data from the osteoarthritis initiative.* Osteoarthritis Cartilage, 2009. 17(12): p. 1562-9.
24. Hawker GA, Stewart L, French MR, Cibere J, Jordan JM, March L, et al., *Understanding the pain experience in hip and knee osteoarthritis--an OARSI/OMERACT initiative.* Osteoarthritis Cartilage, 2008. 16(4): p. 415-22.
25. Neogi T, Felson D, Niu J, Nevitt M, Lewis CE, Aliabadi P, et al., *Association between radiographic features of knee osteoarthritis and pain: results from two cohort studies.* BMJ, 2009. 339: p. b2844.
26. Duncan R, Peat G, Thomas E, Wood L, Hay E, and Croft P, *How do pain and function vary with compartmental distribution and severity of radiographic knee osteoarthritis?* Rheumatology (Oxford), 2008. 47(11): p. 1704-7.
27. Dieppe PA and Lohmander LS, *Pathogenesis and management of pain in osteoarthritis.* Lancet, 2005. 365(9463): p. 965-73.
28. Felson DT, *Osteoarthritis of the knee (vol 354, pg 841, 2006).* New England Journal of Medicine, 2006. 354(23): p. 2520-20.
29. Hunter DJ, Zhang YQ, Niu JB, Goggins J, Amin S, Lavalley MP, et al., *Increase in bone marrow lesions associated with cartilage loss - A longitudinal magnetic resonance imaging study of knee osteoarthritis.* Arthritis and Rheumatism, 2006. 54(5): p. 1529-35.
30. Li G, Ma Y, Cheng TS, Landao-Bassonga E, Qin A, Pavlos NJ, et al., *Identical subchondral bone microarchitecture pattern with increasedbone resorption in rheumatoid arthritis as comparedtoosteoarthritis.* Osteoarthritis and cartilage / OARS, Osteoarthritis Research Society, 2014. 22(12): p. 2083-92.
31. Brandt KD, Dieppe P, and Radin EL, *Etiopathogenesis of osteoarthritis.* Rheumatic diseases clinics of North America, 2008. 34(3): p. 531-59.
32. Kornaat PR, Bloem JL, Ceulemans RY, Riyazi N, Rosendaal FR, Nelissen RG, et al., *Osteoarthritis of the knee: association between clinical features and MR imaging findings.* Radiology, 2006. 239(3): p. 811-7.
33. Kinds MB, Marijnissen AC, Bijlsma JW, Boers M, Lafeber FP, and Welsing PM, *Quantitative radiographic features of early knee osteoarthritis: development over 5 years*

and relationship with symptoms in the CHECK cohort. The Journal of rheumatology, 2013. 40(1): p. 58-65.
34. Javaid MK, Kiran A, Guermazi A, Kwoh CK, Zaim S, Carbone L, et al., *Individual magnetic resonance imaging and radiographic features of knee osteoarthritis in subjects with unilateral knee pain: the health, aging, and body composition study.* Arthritis and rheumatism, 2012. 64(10): p. 3246-55.
35. Amini M, *Stiffness of the Proximal Tibial Bone in Normal and Osteoarthritic Conditions: A Parametric Finite Element Simulation Study*, in *Mechanical Engineering*2013, University of Saskatchewan: Saskatoon.
36. Mcerlain DD, Milner JS, Ivanov TG, Jencikova-Celerin L, Pollmann SI, and Holdsworth DW, *Subchondral cysts create increased intra-osseous stress in early knee OA: A finite element analysis using simulated lesions.* Bone, 2011. 48(3): p. 639-46.
37. Durr HR, Martin H, Pellengahr C, Schlemmer M, Maier M, and Jansson V, *The cause of subchondral bone cysts in osteoarthrosis - A finite element analysis.* Acta Orthopaedica Scandinavica, 2004. 75(5): p. 554-58.
38. Crema MD, Roemer FW, Zhu YY, Marra MD, Niu JB, Zhang YQ, et al., *Subchondral Cystlike Lesions Develop Longitudinally in Areas of Bone Marrow Edema-like Lesions in Patients with or at Risk for Knee Osteoarthritis: Detection with MR Imaging-The MOST Study.* Radiology, 2010. 256(3): p. 855-62.
39. Landells JW, *The Bone Cysts of Osteoarthritis.* Journal of Bone and Joint Surgery-British Volume, 1953. 35(4): p. 643-49.
40. Felson DT, Niu J, Gross KD, Englund M, Sharma L, Cooke TDV, et al., *Valgus malalignment is a risk factor for lateral knee osteoarthritis incidence and progression: findings from the Multicenter Osteoarthritis Study and the Osteoarthritis Initiative.* Arthritis and rheumatism, 2013. 65(2): p. 355-62.
41. Brouwer GM, Van Tol AW, Bergink AP, Belo JN, Bernsen RMD, Reijman M, et al., *Association between valgus and varus alignment and the development and progression of radiographic osteoarthritis of the knee.* Arthritis and rheumatism, 2007. 56(4): p. 1204-11.
42. Sharma L, Chmiel JS, Almagor O, Felson D, Guermazi A, Roemer F, et al., *The role of varus and valgus alignment in the initial development of knee cartilage damage by MRI: the MOST study.* Annals of the rheumatic diseases, 2013. 72(2): p. 235-40.
43. Sharma L, Song J, Felson DT, Cahue S, Shamiyeh E, and Dunlop DD, *The role of knee alignment in disease progression and functional decline in knee osteoarthritis.* Jama, 2001. 286(2): p. 188-95.
44. Fang J, Gong H, Kong LY, and Zhu D, *Simulation on the internal structure of three-dimensional proximal tibia under different mechanical environments.* Biomedical Engineering Online, 2013. 12.
45. Johnston JD, Kontulainen SA, Masri BA, and Wilson DR, *A comparison of conventional maximum intensity projection with a new depth-specific topographic mapping technique in the CT analysis of proximal tibial subchondral bone density.* Skeletal radiology, 2010. 39(9): p. 867-76.
46. Im G-I and Kim M-K, *The relationship between osteoarthritis and osteoporosis.* Journal of bone and mineral metabolism, 2014. 32(2): p. 101-9.

47. Hannan MT, Anderson JJ, Zhang Y, Levy D, and Felson DT, *Bone mineral density and knee osteoarthritis in elderly men and women. The Framingham Study.* Arthritis and rheumatism, 1993. 36(12): p. 1671-80.
48. Nevitt MC, Lane NE, Scott JC, Hochberg MC, Pressman AR, Genant HK, et al., *Radiographic osteoarthritis of the hip and bone mineral density. The Study of Osteoporotic Fractures Research Group.* Arthritis and rheumatism, 1995. 38(7): p. 907-16.
49. Burnett WD, Kontulainen SA, Mclennan CE, Wheaton D, Talmo C, Hunter DJ, et al., *Patella Bone Density Is Lower in Knee Osteoarthritis Patients Experiencing Pain at Rest.* Osteoarthritis and Cartilage, 2012. 20: p. S200-S01.
50. Burnett WD, Kontulainen SA, Mclennan C, Hazel D, Talmo C, Wilson DR, et al., *Proximal tibial trabecular bone mineral density is related to pain in patients with osteoarthritis.* Osteoarthritis and cartilage / OARS, Osteoarthritis Research Society, 2016.
51. Burnett W, *Knee osteoarthritis patients with severe pain while lying down have higher local subchondral tibial bone mineral density*, in *ASBMR*2014.
52. Hulet C, Sabatier JP, Souquet D, Locker B, Marcelli C, and Vielpeau C, *Distribution of bone mineral density at the proximal tibia in knee osteoarthritis.* Calcified Tissue International, 2002. 71(4): p. 315-22.
53. Boyd SK, Matyas JR, Wohl GR, Kantzas A, and Zernicke RF, *Early regional adaptation of periarticular bone mineral density after anterior cruciate ligament injury.* Journal of applied physiology (Bethesda, Md : 1985), 2000. 89(6): p. 2359-64.
54. Li B and Aspden RM, *Material properties of bone from the femoral neck and calcar femorale of patients with osteoporosis or osteoarthritis.* Osteoporosis international : a journal established as result of cooperation between the European Foundation for Osteoporosis and the National Osteoporosis Foundation of the USA, 1997. 7(5): p. 450-6.
55. Li B and Aspden RM, *Composition and mechanical properties of cancellous bone from the femoral head of patients with osteoporosis or osteoarthritis.* Journal of bone and mineral research : the official journal of the American Society for Bone and Mineral Research, 1997. 12(4): p. 641-51.
56. Li B and Aspden RM, *Mechanical and material properties of the subchondral bone plate from the femoral head of patients with osteoarthritis or osteoporosis.* Annals of the rheumatic diseases, 1997. 56(4): p. 247-54.
57. Kamibayashi L, Wyss UP, Cooke TD, and Zee B, *Trabecular microstructure in the medial condyle of the proximal tibia of patients with knee osteoarthritis.* Bone, 1995. 17(1): p. 27-35.
58. Burr DB and Radin EL, *Microfractures and microcracks in subchondral bone: are they relevant to osteoarthrosis?* Rheumatic diseases clinics of North America, 2003. 29(4): p. 675-85.
59. Amini M, Nazemi SM, Lanovaz JL, Kontulainen S, Masri BA, Wilson DR, et al., *Individual and combined effects of OA-related subchondral bone alterations on proximal tibial surface stiffness: a parametric finite element modeling study.* Medical engineering & physics, 2015. 37(8): p. 783-91.
60. Guilak F, *Biomechanical factors in osteoarthritis.* Best practice & research Clinical rheumatology, 2011. 25(6): p. 815-23.

61. Henriksen M, Aaboe J, and Bliddal H, *The relationship between pain and dynamic knee joint loading in knee osteoarthritis varies with radiographic disease severity. A cross sectional study.* The Knee, 2012. 19(4): p. 392-8.
62. Helgason B, Perilli E, Schileo E, Taddei F, Brynjolfsson S, and Viceconti M, *Mathematical relationships between bone density and mechanical properties: A literature review.* Clinical Biomechanics, 2008. 23(2): p. 135-46.
63. Carter DR and Hayes WC, *The compressive behavior of bone as a two-phase porous structure.* The Journal of bone and joint surgery American volume, 1977. 59(7): p. 954-62.
64. Lotz JC, Gerhart TN, and Hayes WC, *Mechanical properties of trabecular bone from the proximal femur: a quantitative CT study.* Journal of computer assisted tomography, 1990. 14(1): p. 107-14.
65. Lotz JC, Gerhart TN, and Hayes WC, *Mechanical properties of metaphyseal bone in the proximal femur.* Journal of Biomechanics, 1991. 24(5): p. 317-29.
66. Snyder SM and Schneider E, *Estimation of mechanical properties of cortical bone by computed tomography.* Journal of orthopaedic research : official publication of the Orthopaedic Research Society, 1991. 9(3): p. 422-31.
67. Hodgskinson R and Currey JD, *Young Modulus, Density and Material Properties in Cancellous Bone over a Large Density Range.* Journal of Materials Science-Materials in Medicine, 1992. 3(5): p. 377-81.
68. Linde F, Hvid I, and Madsen F, *The effect of specimen geometry on the mechanical behaviour of trabecular bone specimens.* Journal of Biomechanics, 1992. 25(4): p. 359-68.
69. Anderson MJ, Keyak JH, and Skinner HB, *Compressive mechanical properties of human cancellous bone after gamma irradiation.* The Journal of bone and joint surgery American volume, 1992. 74(5): p. 747-52.
70. Keller TS, *Predicting the compressive mechanical behavior of bone.* Journal of Biomechanics, 1994. 27(9): p. 1159-68.
71. Keyak JH, Lee IY, and Skinner HB, *Correlations between orthogonal mechanical properties and density of trabecular bone: use of different densitometric measures.* Journal of biomedical materials research, 1994. 28(11): p. 1329-36.
72. Goulet RW, Goldstein SA, Ciarelli MJ, Kuhn JL, Brown MB, and Feldkamp LA, *The relationship between the structural and orthogonal compressive properties of trabecular bone.* Journal of Biomechanics, 1994. 27(4): p. 375-89.
73. Ciarelli MJ, Goldstein SA, Kuhn JL, Cody DD, and Brown MB, *Evaluation of orthogonal mechanical properties and density of human trabecular bone from the major metaphyseal regions with materials testing and computed tomography.* Journal of orthopaedic research : official publication of the Orthopaedic Research Society, 1991. 9(5): p. 674-82.
74. Morgan EF, Bayraktar HH, and Keaveny TM, *Trabecular bone modulus-density relationships depend on anatomic site.* Journal of Biomechanics, 2003. 36(7): p. 897-904.
75. Kaneko TS, Bell JS, Pejcic MR, Tehranzadeh J, and Keyak JH, *Mechanical properties, density and quantitative CT scan data of trabecular bone with and without metastases.* Journal of Biomechanics, 2004. 37(4): p. 523-30.
76. Galante J, Rostoker W, and Ray RD, *Physical properties of trabecular bone.* Calcified tissue research, 1970. 5(3): p. 236-46.
77. Sharp DJ, Tanner KE, and Bonfield W, *Measurement of the density of trabecular bone.* Journal of Biomechanics, 1990. 23(8): p. 853-7.

78. Gibson LJ, *The mechanical behaviour of cancellous bone.* Journal of Biomechanics, 1985. 18(5): p. 317-28.
79. Nazemi SM, Amini M, Kontulainen SA, Milner JS, Holdsworth DW, Masri BA, et al., *Prediction of local proximal tibial subchondral bone structural stiffness using subject-specific finite element modeling: Effect of selected density-modulus relationship.* Clinical biomechanics (Bristol, Avon), 2015. 30(7): p. 703-12.
80. Keyak JH, Rossi SA, Jones KA, and Skinner HB, *Prediction of femoral fracture load using automated finite element modeling.* Journal of Biomechanics, 1998. 31(2): p. 125-33.
81. Austman RL, Milner JS, Holdsworth DW, and Dunning CE, *The effect of the density-modulus relationship selected to apply material properties in a finite element model of long bone.* Journal of Biomechanics, 2008. 41(15): p. 3171-6.
82. Keaveny TM, Pinilla TP, Crawford RP, Kopperdahl DL, and Lou A, *Systematic and random errors in compression testing of trabecular bone.* Journal of orthopaedic research : official publication of the Orthopaedic Research Society, 1997. 15(1): p. 101-10.
83. Mckoy BE, Kang Q, and An YH, *Indentation testing of bone*, in *Mechanical testing of bone and the bone-implant interface*, Y.H. An and R.A. Draughn, Editors. 2000, CRC Press: Boca Raton. p. 233-56.
84. Rho JY, Hobatho MC, and Ashman RB, *Relations of mechanical properties to density and CT numbers in human bone.* Medical engineering & physics, 1995. 17(5): p. 347-55.
85. Kellgren JH and Lawrence JS, *Radiological assessment of osteo-arthrosis.* Annals of the rheumatic diseases, 1957. 16(4): p. 494-502.
86. Kontulainen S, Liu D, Manske S, Jamieson M, Sievanen H, and Mckay H, *Analyzing cortical bone cross-sectional geometry by peripheral QCT: comparison with bone histomorphometry.* Journal of clinical densitometry : the official journal of the International Society for Clinical Densitometry, 2007. 10(1): p. 86-92.
87. Spoor CF, Zonneveld FW, and Macho GA, *Linear measurements of cortical bone and dental enamel by computed tomography: applications and problems.* American journal of physical anthropology, 1993. 91(4): p. 469-84.
88. Vijayakumar V and Quenneville CE, *Quantifying the regional variations in the mechanical properties of cancellous bone of the tibia using indentation testing and quantitative computed tomographic imaging.* Proceedings of the Institution of Mechanical Engineers. Part H, Journal of engineering in medicine, 2016. 230(6): p. 588-93.
89. Carey RE, Zheng L, Aiyangar AK, Harner CD, and Zhang X, *Subject-specific finite element modeling of the tibiofemoral joint based on CT, magnetic resonance imaging and dynamic stereo-radiography data in vivo.* Journal of biomechanical engineering, 2014. 136(4).
90. Kazemi M, Dabiri Y, and Li LP, *Recent advances in computational mechanics of the human knee joint.* Computational and mathematical methods in medicine, 2013. 2013: p. 718423.
91. Gluer CC, Blake G, Lu Y, Blunt BA, Jergas M, and Genant HK, *Accurate assessment of precision errors: how to measure the reproducibility of bone densitometry techniques.* Osteoporosis international : a journal established as result of cooperation between the European Foundation for Osteoporosis and the National Osteoporosis Foundation of the USA, 1995. 5(4): p. 262-70.

92. Burnett WD, Kontulainen SA, Mclennan CE, Hunter DJ, Wilson DR, and Johnston JD, *Regional depth-specific subchondral bone density measures in osteoarthritic and normal patellae: in vivo precision and preliminary comparisons.* Osteoporosis international : a journal established as result of cooperation between the European Foundation for Osteoporosis and the National Osteoporosis Foundation of the USA, 2014. 25(3): p. 1107-14.
93. Mueller TL, Stauber M, Kohler T, Eckstein F, Muller R, and Van Lenthe GH, *Non-invasive bone competence analysis by high-resolution pQCT: an in vitro reproducibility study on structural and mechanical properties at the human radius.* Bone, 2009. 44(2): p. 364-71.
94. Macneil JA and Boyd SK, *Improved reproducibility of high-resolution peripheral quantitative computed tomography for measurement of bone quality.* Medical engineering & physics, 2008. 30(6): p. 792-9.
95. Cann CE and Genant HK, *Precise measurement of vertebral mineral content using computed tomography.* Journal of computer assisted tomography, 1980. 4(4): p. 493-500.
96. Cann CE, *Quantitative CT for determination of bone mineral density: a review.* Radiology, 1988. 166(2): p. 509-22.
97. Muller-Gerbl M, Putz R, Hodapp N, Schulte E, and Wimmer B, *Computed tomography-osteoabsorptiometry for assessing the density distribution of subchondral bone as a measure of long-term mechanical adaptation in individual joints.* Skeletal radiology, 1989. 18(7): p. 507-12.
98. Muller-Gerbl M, Putz R, and Kenn R, *Demonstration of subchondral bone density patterns by three-dimensional CT osteoabsorptiometry as a noninvasive method for in vivo assessment of individual long-term stresses in joints.* Journal of bone and mineral research : the official journal of the American Society for Bone and Mineral Research, 1992. 7 Suppl 2: p. S411-8.
99. Eckstein F, Muller-Gerbl M, and Putz R, *Distribution of subchondral bone density and cartilage thickness in the human patella.* Journal of anatomy, 1992. 180 (Pt 3): p. 425-33.
100. Drum MG, Les CM, Park RD, Norrdin RW, Mcilwraith CW, and Kawcak CE, *Correlation of quantitative computed tomographic subchondral bone density and ash density in horses.* Bone, 2009. 44(2): p. 316-9.
101. Evans FG and Vincentelli R, *Relations of the compressive properties of human cortical bone to histological structure and calcification.* Journal of biomechanics, 1974. 7(1): p. 1-10.
102. Morgan EF and Keaveny TM, *Dependence of yield strain of human trabecular bone on anatomic site.* Journal of biomechanics, 2001. 34(5): p. 569-77.
103. Kopperdahl DL and Keaveny TM, *Yield strain behavior of trabecular bone.* Journal of biomechanics, 1998. 31(7): p. 601-8.
104. Johnston JD, Mclennan CE, Hunter DJ, and Wilson DR, *In vivo precision of a depth-specific topographic mapping technique in the CT analysis of osteoarthritic and normal proximal tibial subchondral bone density.* Skeletal radiology, 2011. 40(8): p. 1057-64.
105. Tuncer M, Hansen UN, and Amis AA, *Prediction of structural failure of tibial bone models under physiological loads: effect of CT density-modulus relationships.* Medical engineering & physics, 2014. 36(8): p. 991-7; discussion 91.

106. Baca V, Horak Z, Mikulenka P, and Dzupa V, *Comparison of an inhomogeneous orthotropic and isotropic material models used for FE analyses.* Medical engineering & physics, 2008. 30(7): p. 924-30.
107. Dar FH and Aspden RM, *A finite element model of an idealized diarthrodial joint to investigate the effects of variation in the mechanical properties of the tissues.* Proceedings of the Institution of Mechanical Engineers Part H, Journal of engineering in medicine, 2003. 217(5): p. 341-8.
108. Henckel J, Richards R, Lozhkin K, Harris S, Rodriguez Y Baena FM, Barrett ARW, et al., *Very low-dose computed tomography for planning and outcome measurement in knee replacement. The imperial knee protocol.* The Journal of bone and joint surgery British volume, 2006. 88(11): p. 1513-8.
109. Cohen J, *Statistical power analysis for the behavioral sciences*, 1988, Erlbaum Hillsdale, NJ.
110. Lin YC, Walter JP, Banks SA, Pandy MG, and Fregly BJ, *Simultaneous prediction of muscle and contact forces in the knee during gait.* Journal of biomechanics, 2010. 43(5): p. 945-52.
111. Al Nazer R, Rantalainen T, Heinonen A, Sievanen H, and Mikkola A, *Flexible multibody simulation approach in the analysis of tibial strain during walking.* Journal of biomechanics, 2008. 41(5): p. 1036-43.